POLITECNICO
MILANO 1863

**SCUOLA DI INGEGNERIA INDUSTRIALE
E DELL'INFORMAZIONE**

Analysis of control system strategies for wind farm performance optimization

TESI DI LAUREA MAGISTRALE IN
ENERGY ENGINEERING - INGEGNERIA ENERGETICA

Author: **Annachiara Frezza**

Student ID: 103409
Advisor: Prof. Alessandro Croce
Co-advisors: Riccardo Riva
Academic Year: 2022-23

Abstract

In the pursuit of maximizing the efficiency of wind farms, particularly in dense configurations where turbines frequently operate in the wakes of others, this thesis explores the integration of advanced control strategies to enhance power production and ultimately reduce energy costs per megawatt, addressing the financial challenges faced by the wind industry nowadays. The thesis employs a detailed methodology involving the `HAWCStab2` tool for aeroservoelastic stability analysis and `PyWake` for wind farm modelling. By first obtaining the regulation trajectory of the chosen reference turbine, namely the IEA 10 MW turbine model, it presents the implementation of the thrust coefficient minimization derating algorithm. Subsequently, the integration of the deratable turbine within the `PyWake` environment is achieved. Lastly, a comparative analysis of different control strategies - derating, wake redirection, and their combination - against a baseline scenario is performed, utilizing the `OpenMDAO` framework for optimization. Findings reveal that the combined strategy promises a potential power production increase of 10% compared to the baseline, albeit with variations based on wind speed.

The research highlights the numerical instability challenges encountered when solely focusing on power maximization and proposes the multi-start method as a solution to identify the global optimum more efficiently. It underscores the need for a holistic approach, suggesting that integrating load minimization objectives could offer a more robust framework for wind farm control strategies.

Keywords: wind farm control, derating, wake redirection, multidisciplinary optimization, `PyWake`

Abstract in lingua italiana

Al fine di massimizzare l'efficienza dei parchi eolici, specialmente nelle wind farm caratterizzate da layout complessi in cui le macchine operano venendo investite dalle scie delle turbine sopravento, questa tesi esplora l'integrazione di strategie di controllo avanzate per potenziare la produzione di energia e, in ultima analisi, ridurre i costi dell'energia eolica per megawatt, così da agevolare i progetti e mitigare le sfide finanziarie che l'industria oggi presenta. La tesi impiega una metodologia dettagliata che coinvolge il software `HAWCStab2` per l'analisi della stabilità aeroservoelastica e `PyWake` per la modellazione di parchi eolici, entrambi sviluppati dal dipartimento di Wind Energy della DTU. Dopo aver ottenuto la traiettoria di regolazione della turbina di riferimento scelta, ovvero il modello IEA 10 MW, lo studio si è posto l'obiettivo di applicare uno specifico algoritmo di derating proposto in letteratura (minimizzazione del coefficiente di spinta) alla suddetta turbina. A seguire, la turbina regolabile è stata integrata all'interno dell'ambiente `PyWake`. La parte consistente del lavoro è stata poi quella di realizzare un'analisi comparativa delle diverse strategie di controllo studiate - derating, deviazione della scia e la loro combinazione - rispetto a uno scenario di base, utilizzando il framework di ottimizzazione multidisciplinare `OpenMDAO`. I risultati rivelano che la strategia combinata promette un potenziale aumento della produzione di energia del 10% rispetto allo scenario di base, sebbene vadano considerate variazioni di tale valore in base alla velocità del vento analizzata. La ricerca evidenzia le sfide di instabilità numerica incontrate quando ci si concentra esclusivamente sulla massimizzazione della potenza e propone il metodo multi-start come soluzione per identificare più efficientemente l'ottimo globale. Viene sottolineata infine la necessità di un approccio olistico, suggerendo che l'integrazione della minimizzazione del carico come obiettivo all'interno del framework di ottimizzazione potrebbe offrire risultati più scientificamente interessanti e spendibili nell'implementazione pratica delle strategie.

Parole chiave: controllo di parchi eolici, derating, deviazione della scia, ottimizzazione multidisciplinare, `PyWake`
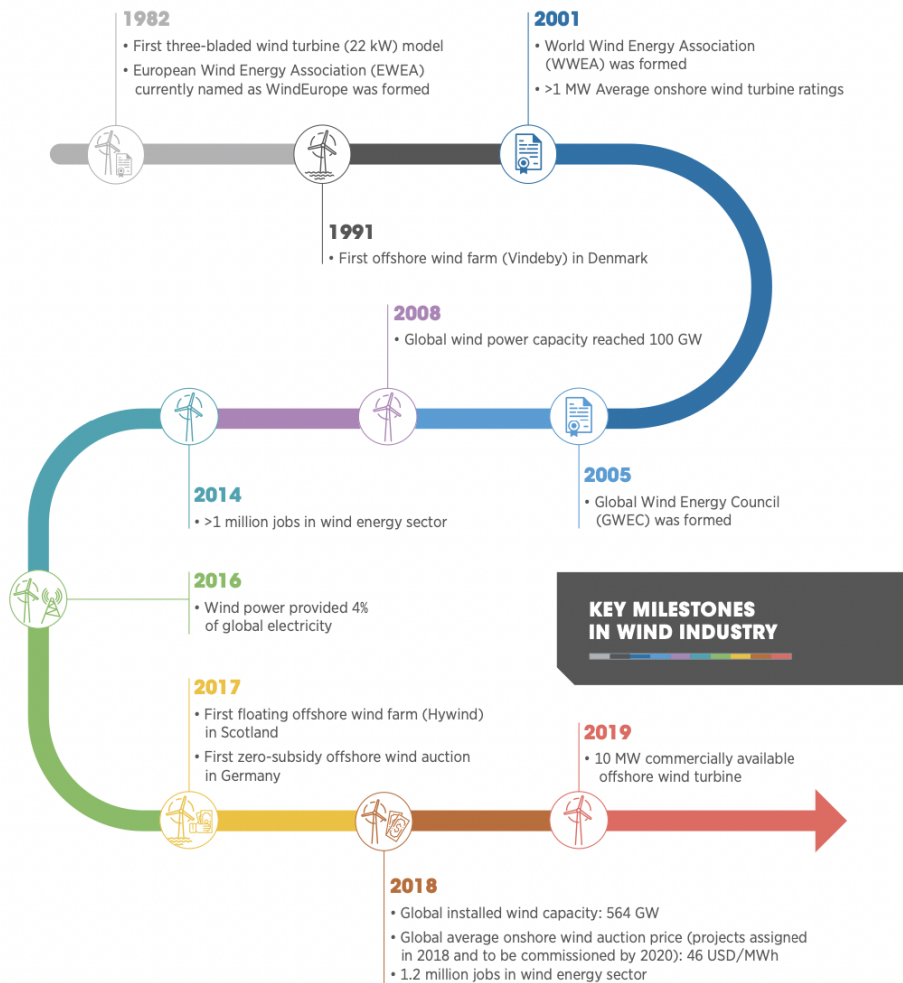
Contents

1 | Introduction

Growing concerns regarding climate change, the adverse health impacts of air pollution, energy security and energy access, coupled with the volatility of oil prices in recent years, have underscored the imperative for developing and adopting alternative, low-carbon technologies like renewables. Among these, wind power has emerged as a pioneering force in the renewable energy landscape over the past few decades (e.g. in Denmark, wind power produced the equivalent of 54.0% of Denmark's total electricity consumption in 2022 [21]), with a significant increase in installed capacity and annual investments over the years [26]. With its total installed capacity ranking third only to hydropower and solar energy, wind power surpassed 900 GW globally by the end of 2022. Notably, alongside solar energy, wind power dominated the additions to total renewable capacity, with approximately 75 GW added worldwide in 2022 according to IRENA [23]. Historically speaking, the trajectory of the wind industry has been remarkable, achieving significant milestones in installations, technological advancements, and cost reductions over the past four decades, alongside the establishment of key wind energy associations (see Fig. 1.1).

1982
- First three-bladed wind turbine (22 kW) model
- European Wind Energy Association (EWEA) currently named as WindEurope was formed

2001
- World Wind Energy Association (WWEA) was formed
- >1 MW Average onshore wind turbine ratings

1991
- First offshore wind farm (Vindeby) in Denmark

2008
- Global wind power capacity reached 100 GW

2014
- >1 million jobs in wind energy sector

2005
- Global Wind Energy Council (GWEC) was formed

2016
- Wind power provided 4% of global electricity

KEY MILESTONES IN WIND INDUSTRY

2017
- First floating offshore wind farm (Hywind) in Scotland
- First zero-subsidy offshore wind auction in Germany

2019
- 10 MW commercially available offshore wind turbine

2018
- Global installed wind capacity: 564 GW
- Global average onshore wind auction price (projects assigned in 2018 and to be commissioned by 2020): 46 USD/MWh
- 1.2 million jobs in wind energy sector

Source: Equinor, 2017; GWEC, 2019a; IRENA, 2019d, 2019e, 2019a, 2019f, 2015; MHI Vestas, 2018; Wind Power Offshore, 2017; WindEurope, 2019a; WWEA, 2015

Figure 1.1: Overview of key milestones achieved by the wind industry since 1982. Figure from [23].

However, the wind industry is currently encountering financial challenges globally, as shown in Fig. 1.2. Major Western manufacturers have recorded losses in the past two years and the wind forecast is less optimistic outside of China. Project development in most countries, aside from China, has progressed slower than anticipated, leading to a downward revision in the onshore wind forecast. In the European Union, lengthy permitting processes, supply chain hurdles, and increased equipment and financial costs are dampening expectations for onshore wind deployment [22].

Renewable electricity capacity forecast revisions, *Renewables 2023* vs *Renewables 2022*
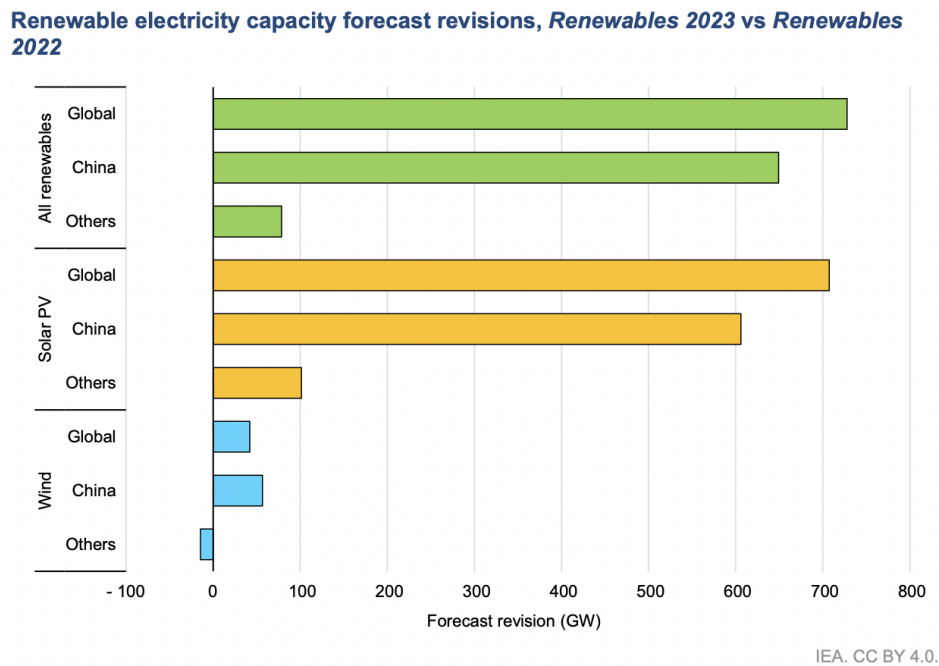
Figure 1.2: The wind forecast is less optimistic outside of China. Figure from [22].

Henceforth, to facilitate the installation of wind energy infrastructure and reverse the trend to which the sector is subject as of 2023, it is essential to investigate strategies aimed at enhancing the operational efficacy of wind farms and their subsequent profitability. Central to easing this process is the reduction of the cost of energy (COE), which is directly linked to the operational control of wind power plants as well as individual wind turbines within them [43]. Contemporary wind farms are equipped with sophisticated monitoring and control technologies to ensure safe and efficient operation, allowing them to meet necessary performance standards. Nevertheless, there is a lack of optimization in balancing competing goals, such as maximizing power output, minimizing turbine loading, and adjusting to spot electricity market prices. As a result, the paradigm of wind farm management is shifting from traditional individual turbine control to a holistic control approach. Consequently, wind farm control has emerged as a field of burgeoning interest, with a substantial body of research being conducted to tackle these critical issues [4].

1.1.   Thesis outline

Chapter 2: Literature review outlines the phenomenon of aerodynamic interaction among wind turbines and presents the most widely used analytical models to assess the wake effect. Lastly, it provides an overview of wind farm control strategies.

Chapter 3: Modeling tools and softwares introduces briefly the reference wind turbine and presents the modeling tools that were employed to develop the work, namely `HAWCStab2` for turbine analysis and `PyWake` for wind farm simulation.

Chapter 4: Methodology describes the foundational steps aimed at introducing the derating control strategy within the wind farm, by firstly adapting the chosen algorithm to the reference turbine and secondly integrating the deratable turbine within the `PyWake` environment.

Chapter 5: Simulations and results presents observations and findings from simulations carried out using derating, yaw-based wake redirection, and their combined effects.

Chapter 6: Conclusions and future developments summarizes the main results and comments on their scientific relevance, while also mentioning the possible developments and improvements this work holds for the future.

2 | Literature review

2.1. Fundamentals of rotor and wind farm aerodynamics

The power production of wind turbines hinges on the interaction between the rotor and the wind, where the latter is typically characterized as a combination of mean wind and turbulent fluctuations. Studies have indicated that key aspects of wind turbine performance, such as mean power output and loads, are primarily influenced by aerodynamic forces generated by the mean wind. Various methodologies have been developed to predict the steady-state performance of wind turbine rotors, with classical analyses pioneered by Betz and Glauert in the 1930s and later refined for digital computation. These approaches combine momentum theory and blade element theory into a strip theory, allowing for the calculation of rotor performance characteristics [2].

A simple model, generally attributed to Betz (1926), can be used to determine the power from an ideal turbine rotor, the thrust of the wind on the ideal rotor, and the effect of the rotor operation on the local wind field [2]. In order to conduct the analysis, it is necessary to consider a control volume whose boundaries are the surface and the two cross-sections of a stream tube. The turbine is thus represented by a thin and uniform "actuator disk", which creates a discontinuity of pressure in the air flowing through it, as shown in Fig. 2.1.
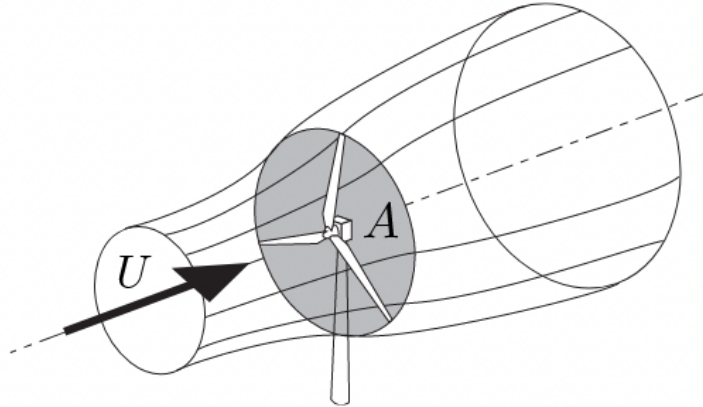
Figure 2.1: Flow with velocity U [m/s] through a rotor disk with rotor swept area A [m^2]. Figure from [8].

The following discussion is adapted from [2].

From the conservation of linear momentum for a one-dimensional, incompressible, steady flow, the thrust T is equal and opposite to the rate of change of momentum of the air stream:

$$T = U_1(\rho A U)_1 - U_4(\rho A U)_4 \tag{2.1}$$

where ρ is the air density, A is the cross-sectional area, U is the air velocity, and the subscripts indicate values at numbered cross-sections in fig. 2.2.
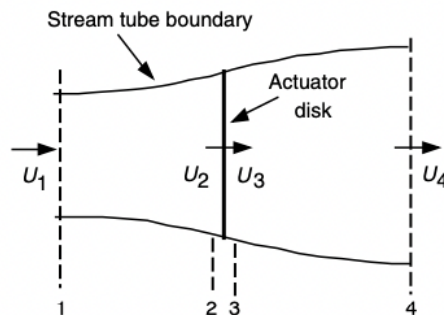

Figure 2.2: Actuator disk model: 1,2,3 and 4 indicate locations. Figure from [2].

Since for steady-state flow $\dot{m} = (\rho A U)_1 = (\rho A U)_4$ (continuity equation [28]), equation 2.1 becomes:

$$T = \dot{m}(U_1 - U_4) \tag{2.2}$$

With further manipulations and applying the Bernoulli theorem, the power output of the

rotor is equal to thrust times the velocity at the disk $U_2 = \frac{U_1+U_4}{2}$:

$$P = \frac{1}{2}\rho A_2(U_1^2 - U_4^2)U_2 \tag{2.3}$$

Finally, with the introduction of the axial induction factor which is a measure of the decrease in wind velocity behind a wind turbine, $a = \frac{U_1-U_2}{U_1}$, the power can be expressed as follows:

$$P = \frac{1}{2}\rho AU^3 4a(1-a)^2 \tag{2.4}$$

where the rotor area A_2 and the free stream velocity U_1 are substituted with A and U, respectively.

To quantify the extracted power with respect to the available power in the wind and thus to assess the turbine rotor performance, the power coefficient C_P is defined:

$$C_P = \frac{P}{\frac{1}{2}\rho AU^3} \tag{2.5}$$

The theoretical limit for energy extraction by a rotor is represented by the Betz limit, determined by taking the derivative of the power coefficient with respect to a and setting it equal to zero, yielding $a = \frac{1}{3}$. Thus:

$$C_{P,max} = 0.5926 \tag{2.6}$$

Similarly, the thrust coefficient C_T is the ratio of the thrust force to the dynamic pressure:

$$C_T = \frac{\frac{1}{2}\rho AU^2[4a(1-a)]}{\frac{1}{2}\rho AU^2} \tag{2.7}$$

Fig. 2.3 shows that the maximum value of C_T occurs at $a = 0.5$ and that this idealized model is not valid for axial induction factors greater than 0.5 because it would mean that the wind speed behind the rotor (U_4) has slowed down to zero velocity.
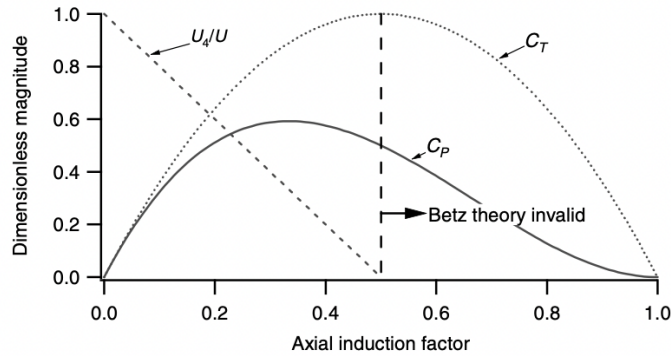
Figure 2.3: Operating parameters for a Betz turbine. Figure from [2].

2.2.   Aerodynamic interaction

Since the pioneering works of Betz and Joukowsky, significant research has been devoted to wind turbine aerodynamics, particularly in optimizing horizontal axis wind turbine (HAWT) rotors. Glauert (1935) made a breakthrough with the formulation of the blade element momentum (BEM) theory, which serves as the foundation for modern rotor de-sign optimization codes. These advancements have enabled modern HAWTs to achieve power coefficients close to the theoretical Betz–Joukowsky limit of 0.593 [37]. However, the prediction of wind-turbine and wind-farm performance is hindered by the complex interactions between wind turbines and the atmospheric boundary layer (ABL), which is highly turbulent, non-stationary, modulated by ubiquitous thermal effects, and often heterogeneous [37]. As a result, improving the understanding of ABL-turbine dynamics holds the potential to enhance the economic viability of wind-energy projects.

Wind turbines are frequently clustered together within wind farms due to their economic advantages.[1] However, as each turbine generates a wake, time-varying interactions arise, resulting in diminished wind speed and higher turbulence for the downstream turbine. Traditionally, industry practices involved controlling turbines individually, thus disre-garding these interactions and ultimately leading to suboptimal performance of the entire wind farm. Consequently, there has been a growing emphasis on wind farm control in recent years, aimed at enhancing total power production and reducing dynamic turbine loading [8].

In other terms, the study of the "wake effect" and the advancement of wind-farm control represent key enablers for the development of large wind farm projects and their safe and efficient connection to the power grid [4].

---

[1]Guidelines are provided for wind turbine spacing in a wind farm [11].

2.2.1. Wake modeling

The concept of aerodynamic coupling is illustrated in Fig. 2.4, where two wind turbines are aligned with the incoming wind. The interaction between the blades of Turbine 1 and the incoming wind generates a downstream airflow region characterized by reduced velocity and increased turbulence intensity, known as a wake [26, 31]. Turbine 2, positioned in the wake generated by Turbine 1, consequently experiences decreased power production and accumulates greater fatigue damage over time. This phenomenon, commonly known as the wake effect, can lead to a reduction in power production from individual downstream turbines by up to 60%, and diminish the overall power output from a wind farm by as much as 54% [26, 35]. Annually, the wake effect may result in cumulative revenue losses ranging from 20 to 30% [10].
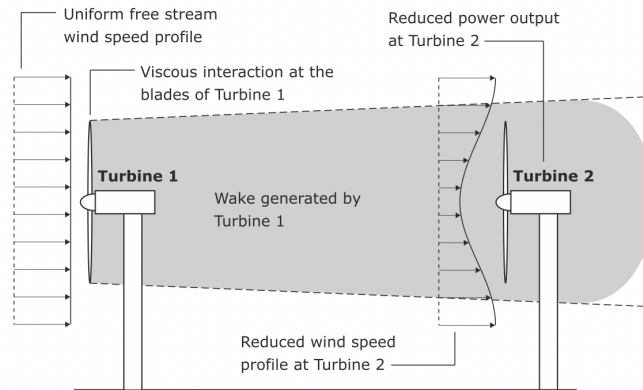

Figure 2.4: The phenomenon of aerodynamic coupling between two wind turbines aligned with the free stream wind. Figure from [26].

The upwind region of a turbine is referred to as the induction region, whereas the downwind flow is distinguished into a near wake and a far wake, as shown in Fig. 2.5 [2].
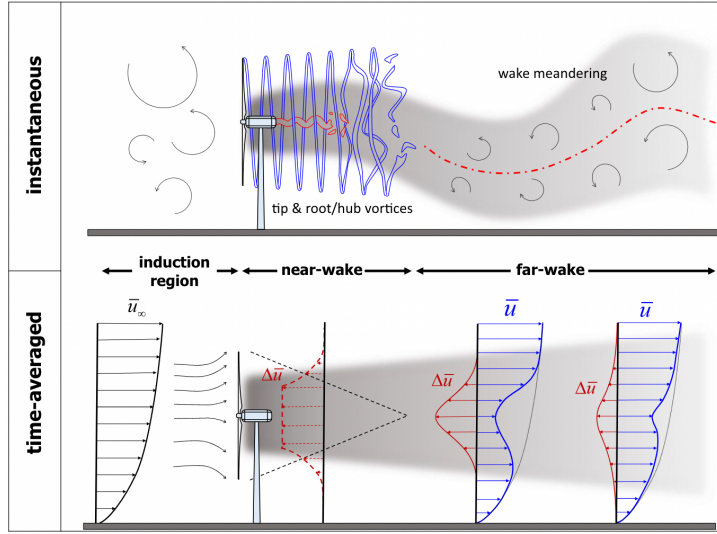
Figure 2.5: The most characteristic instantaneous (top) and time-averaged (bottom) flow features. Figure from [37].

Induction region

The main impact of the turbine on this region is a reduction in wind speed, the so-called "blockage effect", which can be estimated acceptably with the following simple relationship based on the vortex sheet theory [32, 37]:

$$\frac{\bar{u}}{\bar{u}_\infty} = 1 - a\left(1 + \frac{2x}{d}\left(1 + \left(\frac{2x}{d}\right)^2\right)^{-0.5}\right) \tag{2.8}$$

where u is the streamwise velocity component along the rotor axis (the overbar denotes time averaging), x is the streamwise position (being zero at the turbine and negative upwind), u_∞ is the streamwise velocity component far upwind, d is the rotor diameter, and a is the rotor induction factor.

Near wake

The near wake is directly influenced by the presence of the wind turbine, so characteristics of the turbine, such as the blade profile, hub and nacelle geometry, can affect the flow field in this region [11, 37]. As a result, the near-wake is characterized by highly complex, three-dimensional and heterogeneous flow distribution.

Far wake

The far-wake area is less affected by specific wind turbine characteristics. Instead, general parameters of wind turbines, such as thrust and power coefficients, along with incoming flow conditions, are typically sufficient to forecast the average flow distribution in this zone [37].

Globally, the wake effect comprises the following phenomena [8]:

- Wind velocity deficit, because of the turbine's energy extraction;

- Increased turbulence intensity, for i.a., the turbine blade's rotation;

- Wake recovery, namely the acceleration to free-stream velocity due to mixing;

- Wake meandering, represented by horizontal and vertical oscillations over time;

- Wake expansion, explained by the law of mass conservation and flow incompressibility assumptions;

- Wake deflection, due to blade rotations or yawed/tilted condition of the turbine.

2.2.2. Engineering wake models

As mentioned earlier, the wake generated by an upwind turbine plays a crucial role in affecting the performance of downwind turbines. The primary goal of wind farm modeling and control is to consider these interactions and utilize control parameters to achieve desired performance levels. One approach involves incorporating the nonlinear stochastic behavior into a mathematical model, which is then used to devise a controller ensuring specific performance outcomes. The underlying assumption is that implementing this controller in a real wind farm will yield performance consistent with what was predicted by the model used for controller development. However, the effectiveness of this approach hinges on the accuracy and reliability of the model. This highlights a major challenge in wind farm modeling and control: comprehending wake dynamics and capturing the essential interactions within the wake. In the following paragraphs four analytical wake models are described, highlighting their physical modeling capabilities and their empirical parameter dependencies, as well as two commonly used deflection models [8].

The most relevant parameter to take into account when analyzing a wake is the streamwise velocity u [18], expressed as:

$$u = u_\infty(1 - \delta u) \qquad (2.9)$$

where δu is the streamwise velocity deficit caused by the wake effect with respect to the

mean freestream velocity u_∞. While the phenomenon under analysis is three-dimensional and time-variant, all the models presented neglect time dependency and consider space dependency only. For a graphic representation of the described models and to catch the differences amongst them, refer to 2.6.
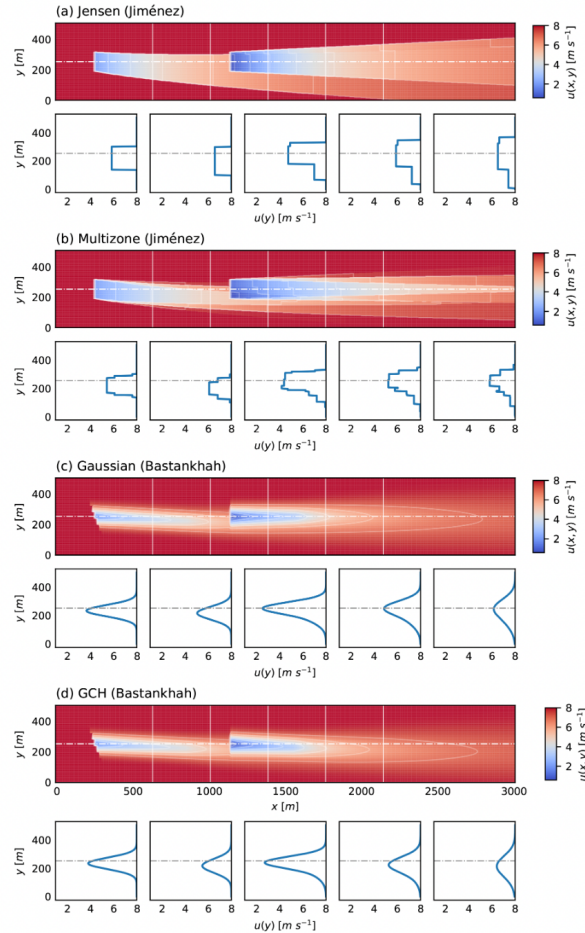

Figure 2.6: Streamwise velocity at hub height of a 2×1 wind farm layout for the discussed wake and deflection models at an upstream rotor yaw angle of 20°. The white vertical lines represent the streamwise locations for the velocity profile section plots, ordered by increasing downstream distance, while the horizontal lines indicate the upstream rotor centerline. Figure from [18].

Jensen model

The Jensen model (1983) is a simple, steady wake model which relies on two assumptions: the conservation of the cross-stream integral of the streamwise velocity deficit as the wake linearly expands downstream and the velocity deficit simply being a function of the

downstream distance x [18]. Therefore, δu can be expressed as:

$$\delta u(x,r) = \begin{cases} 2a\left(\frac{D}{D+2kx}\right)^2, & \text{if } r \leq \frac{D}{D+2kx} \\ 0, & \text{otherwise} \end{cases}$$

with r and x being the cylindrical coordinates of a reference system having its origin placed at the rotor hub of the wake emitting turbine. The wake is parameterized by a tuneable nondimensional wake decay constant, k. Typical values of k range from 0.01 to 0.5 depending on ambient turbulence, topographical effects, and turbine operation [5].
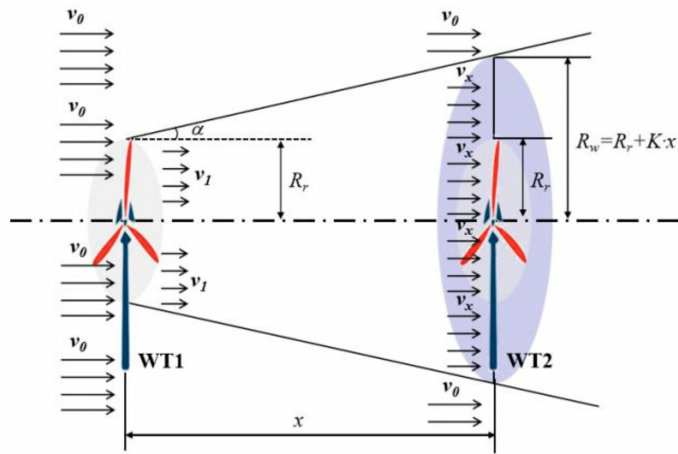

Figure 2.7: Schematic of Jensen's wake model. Figure from [40].

Despite its limitations, including i.a. the disregard of added turbulence intensity and its restricted validity in the far-wake region, the Jensen model remains extensively employed in control and optimization studies, thanks to its simplicity and computational efficiency.
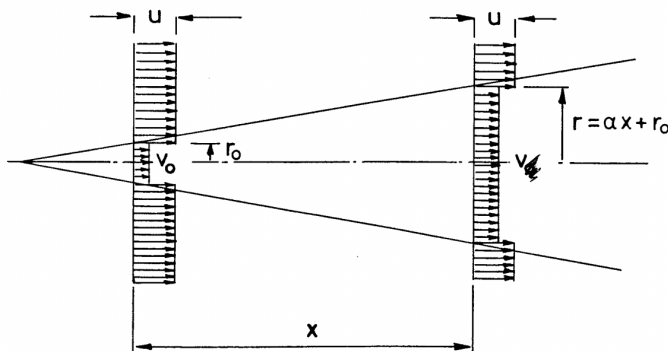

Figure 2.8: Original schematic of Jensen's wake model from 1983. Figure from [24].

Multizone model

Developed by Gebraad et al. (2014), the multizone model extends the validity of the Jensen model to yawed conditions, by taking into account partial wake overlapping. Within a turbine wake, three zones q are defined: near-wake zone (q = 1), far-wake zone (q = 2), and mixing-wake zone (q = 3). They are assumed to expand linearly with downstream distance x [18].

This model is suitable for control and optimization studies, including yaw applications. Nevertheless, other than presenting the same limitations as the Jensen model (it does not have any sensitivity to turbulence intensity and does not explicitly conserve momentum), it also requires the tuning of thirteen empirical parameters, hindering its confidence across operating conditions [5].

Gaussian model

The Gaussian wake model was originally developed by Bastankhah and Porté-Agel (2014) and has recently been improved by various studies in the literature [18]. This steady wake model consists of a mass- and momentum-conserving formulation based on a simplification of the Navier–Stokes equations, and includes a Gaussian wake to describe the velocity deficit, added turbulence based on turbine operation, and atmospheric stability [5].

Despite the increased complexity of the wake model, the Gaussian wake model remains applicable for control and optimization purposes. It incorporates considerations such as ambient and added turbulence intensity and explicitly conserves momentum within the wake. However, there are notable limitations, including its formulation based on a free shear approximation of the Navier–Stokes equations and its tendency to provide inaccurate predictions in the near wake. The Gaussian model was included as a wake model within `FLORIS` and `PyWake` tools. It has been used to design a controller for a field campaign in Fleming et al. (2019) and study wake steering robustness (Simley et al., 2019), and it has been validated with lidar measurements (Annoni et al., 2018) [27].

Gaussian-curl hybrid model (GCH)

The GCH model was first described in King et al. (2021). It was described as a combination of the Gaussian model detailed in Bastankhah and Porté-Agel (2014, 2016) and Niayifar and Porté-Agel (2015) with an approximation of the curl model of wake steering first presented in Martínez-Tossas et al. (2019) [7]. It accounts for yaw-induced wake recovery and secondary steering observed in extensive arrays of turbines during wake steering implementation, contrasting with the Gaussian model, which focuses solely on the aero-

dynamic interaction of wake steering between two turbines. Turbines operating with yaw misalignment generate counter-rotating vortices that capture momentum and contribute to the alteration and redirection of the wake downstream. Arrays of turbines can amplify the impact of wake steering, benefiting turbines located further downstream. This model quantifies these effects and illustrates that wake steering holds significant potential to enhance wind farm performance, particularly in the presence of these counter-rotating vortices, especially for extensive turbine arrays [27]. It was proposed as a compromise which maintains the many advantages of the Gaussian model while incorporating corrections to address the following three important discrepancies [27]:

1. Vortices initiate a mechanism of enhanced wake recovery through yaw adjustment, resulting in improved alignment with Large-Eddy Simulation (LES) and field observations.

2. The interplay between counter-rotating vortices and the shear layer of the atmospheric boundary layer, along with wake rotation, naturally generates wake asymmetry.

3. Incorporating vortex modeling allows for the consideration of secondary steering and associated multi-turbine interactions, a crucial aspect for assessing wake steering in extensive wind farm setups.
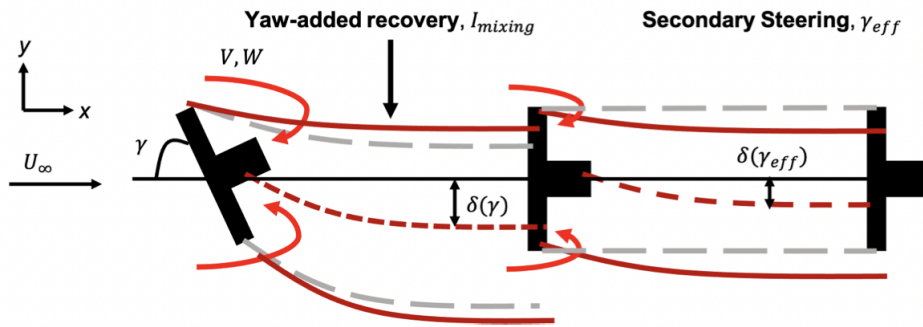

Figure 2.9: Model setup that includes yaw-induced effects such as yaw-added recovery and secondary steering. The standard modeling for wake deflection is shown in gray, and the proposed deflection model in [27] is shown in red. Figure from [27].

2.2.3.   Deflection models

Jiménez model

Deflection models are used to derive the so-called "skew angle" by which the stream is deflected with respect to the ambient air velocity when turbines are not aligned with the incident wind.
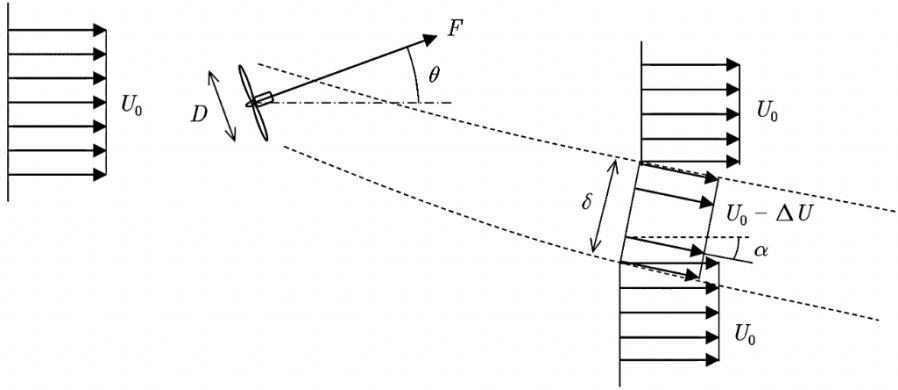

Figure 2.10: Schematic showing of the Jiménez deflection model. Figure from [25].

In this particular model developed by Jiménez and Crespo in 2009, the main assumptions are [18]:

1. The streamwise velocity deficit values are almost negligible compared with inflow velocity $u_\infty - \delta u \simeq u_\infty$.

2. The wake skew angle α is small enough that $\cos(\alpha) \approx 1$ and $\sin(\alpha) \approx \alpha$.

Therefore, the value of α can be derived as a function of δ, the wake width, comparing the equations that allow to compute the projection of the force exerted by the turbine on the flow in the incident wind direction and that aligned with the horizontal direction perpendicular to it. Consequently:

- if $\delta \approx D$, $\alpha|_{x=0} = \cos^2(\theta)\sin(\theta)\frac{C_T}{2}$

- if $\delta = D + \beta x$, $\alpha \approx \frac{\cos^2(\theta)\sin(\theta)\frac{C_T}{2}}{(1+\beta\frac{x}{D})^2}$

However, the model is valid only in the far-wake region where the wake spread is ruled by the ambient turbulence. Furthermore, the specification of β is subject to the adopted literature (e.g. Vermeulen, Lissaman, Katic et al. and Voutsinas et al.) [25].

Bastankhah model

The Bastankhah deflection model, derived from a budget analysis of the continuity and Reynolds-averaged Navier-Stokes equations by Bastankhah and Porté-Agel (2016), utilizes vortex theory to determine wake deflection angles. The model defines the wake deflection angle at the rotor and extends it to the near-wake region, approximating near-wake deflection as a constant value. This allows for the expression of far-wake onset wake deflection. The total far-wake deflection due to wake steering is then calculated, considering factors such as turbine operating conditions, ambient and added turbulence intensity. The model, however, lacks considerations for asymmetry due to wake rotation, vertical and cross-stream velocity components, and wake meandering [18].

2.3. Wind farm control

While placing turbines together offers benefits such as reduced setup expenses for both the turbines and the electrical grid, along with diminished operational costs and environmental impact, challenges arise when turbines operate in proximity [8], because of the wake effect earlier described. This issue can be addressed mainly in three ways [26]:

1. increasing the inter-turbine spacing, in order to re-energize the wake and mitigate the velocity deficit;

2. optimizing the wind farm layout and siting the turbines such that the annual energy production is maximized, by combining engineering wake models and optimization algorithms;

3. adopting wind farm control.

The first two approaches, while beneficial, may contradict the core purpose of wind farms, that is to aggregate turbines closely to minimize both capital and operational costs. Additionally, these modifications cannot be implemented in existing wind farms. Wind farm control, conversely, can be applied to operational farms irrespective of their existing layout, whether it is gridded or has been optimized. Essentially, wind farm control leverages real-time data to fine-tune control strategies, aiming to optimize the efficiency of the wind farm by reconciling the benefits of close turbine placement with the negative effects of wake interaction.

This section will delve into the objectives and challenges of wind farm control, examining strategies like wake steering and axial induction control to coordinate turbine operations, ultimately to uplift power production and extend turbine longevity while fostering a

seamless integration of wind energy into the market.

2.3.1. Objectives of wind farm control

A wind farm controller manages the operation and energy output of each wind turbine within the farm by employing the available degrees of freedom, impacting the overall power production, wind flow, and turbine interactions, as well as influencing turbine fatigue. The primary goals pursued by a wind farm controller encompass the following: enhancing overall energy generation, reducing mechanical loads, complying with electrical grid requirements while offering ancillary services[2], and addressing disturbances and failures caused by external factors [4].
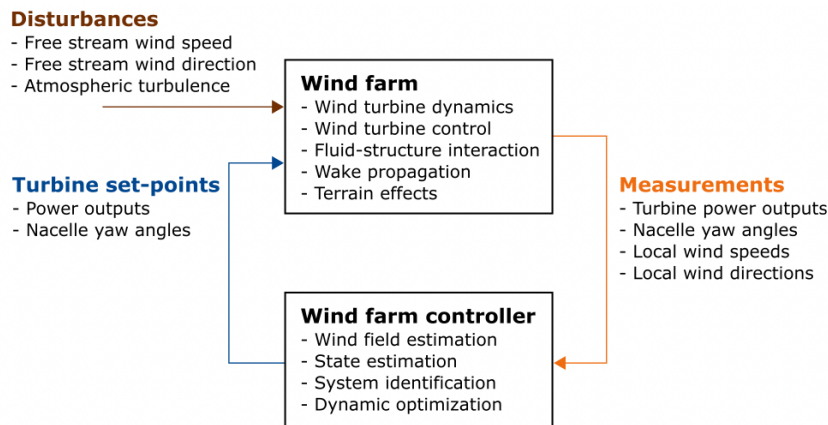
Figure 2.11: The closed-loop feedback structure of a general control system for wind farm power maximization. Figure taken from [26].

Power production maximization

The objective of maximizing power production within a wind farm addresses the inherent challenge posed by the wake effect (refer to Section 2.2 on page 8), where wind turbines extract momentum from the airflow, leading to a velocity deficit in the downstream turbines' wake [8]. Research has shown that losses can range from approximately 25% in turbines spaced 16 rotor diameters apart to as much as 80% when the spacing is reduced to just 4 rotor diameters [8, 17]. These figures underline the critical importance of accurately modeling and predicting wake effects, as the choice of model and methodology can greatly influence the estimated losses. Despite the variability in predictions, the consensus on the substantial impact of wake effects in power production underscores its significance as a key area of focus in wind farm control research.

---

[2]This type of control is called active power control (APC) and will not be discussed in this section.

Load minimization

The loads an upwind horizontal axis wind turbine is subject to are [8]:

- Gravitational loads, which are related to the gravitational field and cause a sinusoidal loading on the blades with a frequency corresponding to the rotor rotation of once per revolution (1P);

- Inertial loads, which arise with rotor speed variations;

- Aerodynamical loads, that occur with the natural variation in time and space of the wind flow.

The goal of single turbine control is to mitigate gravitational, inertial, and aerodynamic loading impacts. At the wind farm control level, the focus shifts towards managing changed aerodynamic loading due to upwind turbines. The Damage Equivalent Load (DEL) metric[3] is commonly utilized in literature for quantifying loading, facilitating direct quantitative comparisons of different loading impacts on turbine structures.

2.3.2. Control strategies

The following paragraphs are dedicated to the description of the most commonly studied control techniques, in order to provide the reader with a clear understanding of what they imply.

---

[3]It calculates the equivalent fatigue damage caused by a load, considering the material's fatigue characteristics.
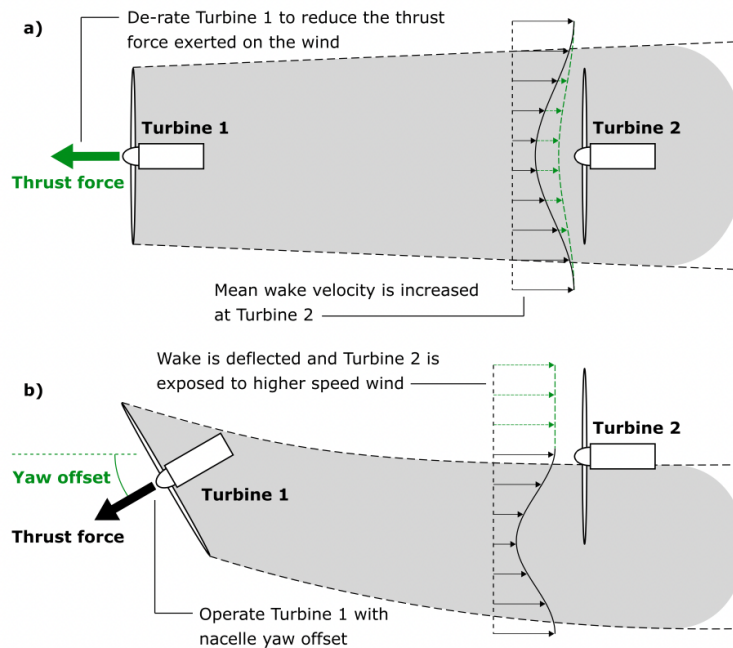
Figure 2.12: Graphical representation of derating and wake redirection. Green elements highlight changes in turbine operation and wake conditions. Figure adapted from [26].

Power derating

The most traditional and widely discussed strategy in the literature, initially introduced by Steinbuch in 1988, centers on power derating, also known as axial induction-based control (AIC). Axial induction refers to the reduction in air momentum as it passes through a wind turbine, closely linked to the turbine's power and thrust coefficients. As depicted in Fig. 2.12, decreasing the power output of Turbine 1 by lowering its axial induction factor reduces both its power generation and the overall thrust force exerted on the wind by its rotor [26]. This adjustment can be carried out by controlling the generator torque or the pitch angle. Consequently, Turbine 2, positioned downstream within this modified wake, encounters higher wind speeds, thereby increasing its electrical output compared to a scenario where Turbine 1 operates at full capacity. This approach is theoretically effective because the power increment at Turbine 2 can compensate for the power reduction at Turbine 1, given a suitable level of power derating. Using only axial induction control often falls short of making a notable impact on power output. However, its potential for reducing loads makes it a compelling option and a viable way method for managing wake effects.

Wake redirection

Wake redirection (WR), or wake steering, consists in misaligning the upstream rotor from the incoming wind to deflect the wake downstream, so that it will not at all or partially overlap a downwind turbine [8]. As illustrated in Fig. 2.12, applying a nacelle yaw offset to Turbine 1 redirects its wake in the yaw direction. This redirection diminishes the overlap between the deflected wake and Turbine 2's rotor, exposing parts of Turbine 2 to faster, less wake-disturbed wind. This control technique can be performed through:

- Tilt actuation;

- Individual pitch control (IPC);

- Yaw actuation.

In the present work, only yaw-based WR will be analyzed.

Benefits and drawbacks

In conclusion, it is essential to highlight the advantages and challenges associated with the control strategies discussed with respect to the wind farm control objectives. Specifically, wake redirection has emerged as a superior method for enhancing power output compared to axial induction control [6]. Nonetheless, accurately determining the effect of wake redirection on turbine loading is complex, as it varies with multiple factors like wind speed, turbulence intensity, and the presence of a shear layer. Studies indicate that extended yaw misalignment can effectively reduce cyclic loads on turbines situated downstream of those operating off-axis. However, the impact on turbines upstream is more ambiguous, potentially offering both positive and negative outcomes depending on the specific turbine component involved [13]. Moreover, many existing wind farms were not initially designed to accommodate the potential load increases from such consistent skewed-inflow operations, necessitating careful consideration when implementing this control approach [12].

3 | Modeling tools and softwares

3.1. Reference wind turbine and farm

A simple wind farm consisting of two IEA 10-MW offshore wind turbines has been considered for this thesis. The turbine's main features are reported in Table 3.1.

Parameter	Value
Wind regime	IEC class 1A
Rated electrical power	10 MW
Rotor orientation	Clockwise rotation - Upwind
Control	Variable Speed Collective Pitch
Rotor diameter	198.0 m
Hub diameter	4.6 m
Hub height	119.0 m
Cut-in wind speed	4 m/s
Cut-out wind speed	25 m/s
Rated wind speed	11 m/s
Airfoil series	FFA-W3
Minimum rotor speed	6.0 rpm
Maximum rotor speed	8.68 rpm
Drive-train	Direct-drive
Rated torque	11.704 MNm
Gearbox ratio	N/A
Maximum tip speed	90.0 m/s
Hub overhang	7.1 m
Shaft tilt angle	6.0 deg
Rotor precone angle	4 deg
Blade prebend	6.2 m
Blade mass	47,700 kg
Nacelle mass	542.600 kg
Tower mass	628,442 kg

Table 3.1: IEA 10-MW reference turbine main parameters.

The overall characteristics of the offshore turbine designed for the IEA Wind Task 37 were based on the feedback gained from the many users of the DTU 10-MW RWT, with respect to which IEA 10-MW was designed [9].
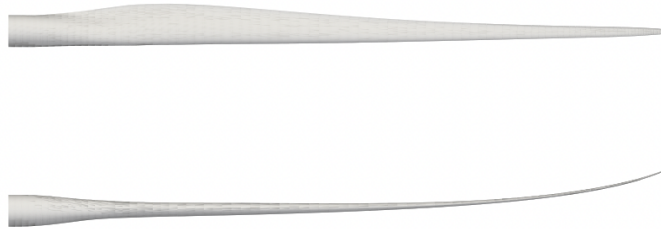

Figure 3.1: View from the pressure side and from the leading edge of the offshore wind turbine blade. Figure from [9].
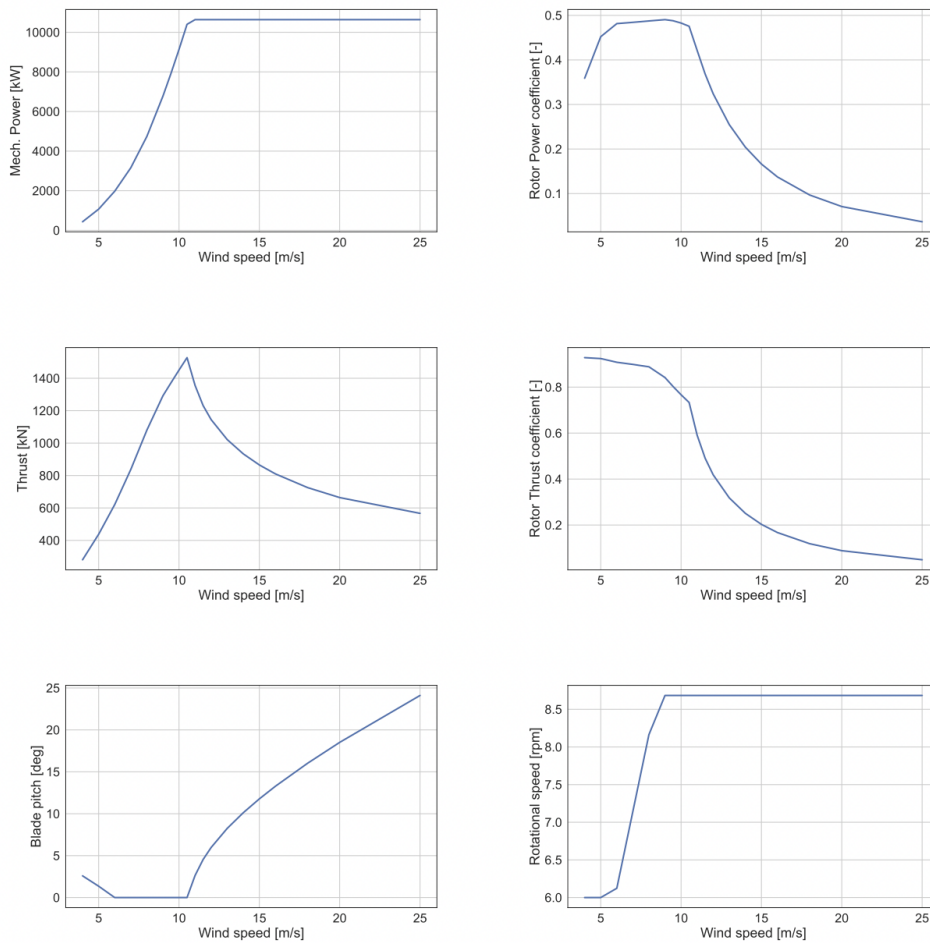

Figure 3.2: Steady-state performance and operation of the 10-MW rotor. Figure from [9].

Wind speed	Pitch	RPM
[m/s]	[deg]	[-]
4.00	2.589	6.000
5.00	1.355	6.000
6.00	0.000	6.123
7.00	0.000	7.144
8.00	0.000	8.165
9.00	0.000	8.684
9.50	0.000	8.684
10.00	0.000	8.684
10.50	0.000	8.684
11.00	2.633	8.684
11.50	4.537	8.684
12.00	5.975	8.684
13.00	8.250	8.684
14.00	10.121	8.684
15.00	11.771	8.684
16.00	13.280	8.684
18.00	16.018	8.684
20.00	18.513	8.684
25.00	24.110	8.684

Table 3.2: Operational data of the 10-MW rotor [9].

3.2. Wind turbine modeling through aero-servo-elastic stability tool HAWCStab2

The tool used in the present thesis is `HAWCStab2`, a frequency-based aero-servo-elastic code designed for steady-state computation and stability analysis of wind turbines. `HAWCStab2` employs an analytical linearization of a nonlinear finite element beam model coupled with an unsteady blade element momentum model, accounting for shed vorticity, dynamic stall, and dynamic inflow.

In his work [19], Hansen et al. present a comprehensive framework for aeroelastic modeling of a single blade using `HAWCStab2`, in which the kinematics is rendered via a corotational formulation to model large displacements and rotations. They represent the blade's structure using discrete two-node prismatic Timoshenko elements, allowing for both displacements and rotations at the second node of each element, which therefore has six degrees of freedom. The IEA 10-MW reference turbine is modeled through 19 elements [1].
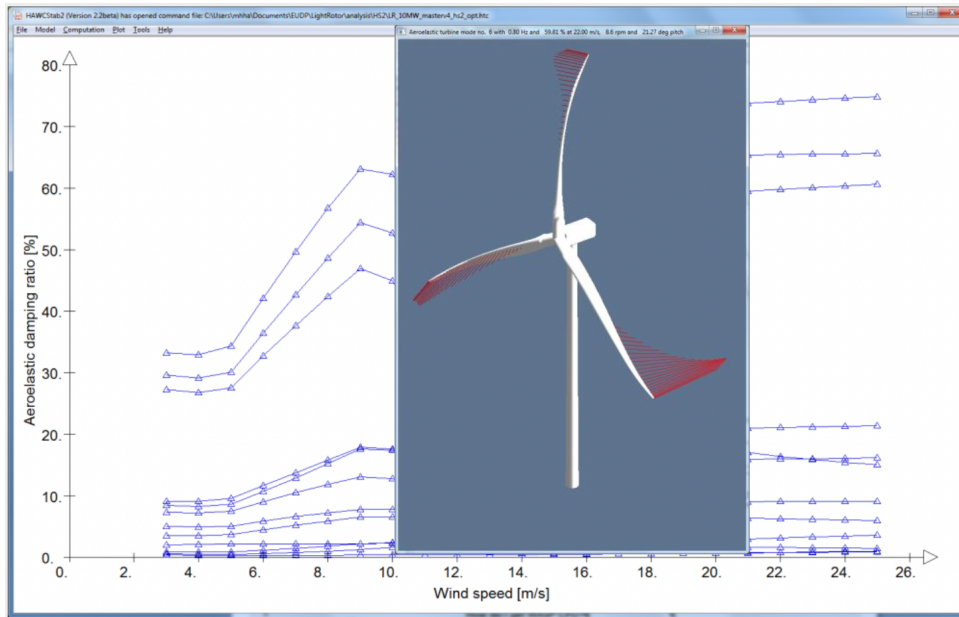
Figure 3.3: The graphical user interface of `HAWCStab2` shows a calculation of aeroelastic damping for a wind turbine versus operational wind speed. Figure from [14].

The modeling process employs a detailed nonlinear iterative procedure to compute steady-state blade deflection by balancing internal blade forces against external aerodynamic forces, laying the groundwork for linear eigenvalue analysis of small vibrations around this steady state. It specifies the position of the elastic axis and the rotation of a cross-section along the blade within the blade frame. Additionally, aerodynamic calculation points are defined along the blade span to derive relative inflow velocities, accounting for steady-state axial and tangential velocities induced by the wake, thus enabling accurate modeling of aerodynamic forces. The equations of motion, derived from Lagrange's equations, incorporate kinetic and potential energies, Rayleigh's dissipation function for structural damping, and generalized forces due to non-conservative aerodynamic forces.

3.3. Wind farm modeling through PyWake

`PyWake` [36] is the DTU open-source tool designed to calculate Annual Energy Production (AEP) for wind farms, akin to `FLORIS` [3], both sharing a modular structure and the ability to be employed in wind farm optimization. `PyWake` has been crafted using an object-oriented approach, emphasizing modularity and computational efficiency achieved through widespread application of vector operations. At the core of `PyWake`'s architecture lies the `WindFarmModel`, initialized with `Site` and `WindTurbines` objects. The `WindFarmModel` returns a `SimulationResult` object containing relevant parameters such as effective wind

speed, power production, and thrust coefficient for individual turbines. Additionally, `PyWake` provides methods for AEP calculation and flow map generation for entire wind farms [15]. The main objects, as depicted in Figure 3.4, are summarized below.

`Site` This component provides local wind speed, wind direction, turbulence intensity, and probability for each point based on a given reference wind speed and direction. It has the capability to simulate both flat and complex terrains [38].

`WindFarmModel` Within `PyWake`, a suite of predefined wind farm models encompasses all engineering models integrated from existing literature and tailored to `PyWake`'s functionalities. Each model is equipped with default configurations for wake deficit, superposition, and turbulence models. Nonetheless, these settings are highly adaptable, allowing for thorough exploration of the effects of different modeling approaches on the outcomes [15].

`WindTurbines` This component determines the power and thrust coefficient of each wind turbine [38].

`AEPCalculator` This component determines the AEP by aggregating the power output of each turbine across various wind speeds and directions, weighting them by their corresponding probabilities [38].
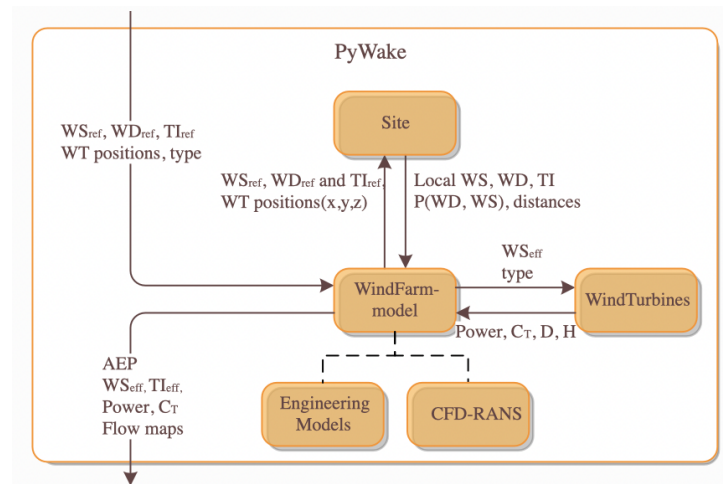
Figure 3.4: Architecture of `PyWake`. Figure from [15].

3.3.1. Engineering Wind Farm Models

As mentioned above, wind farms models are inherited from from two base classes: `PropagateDownwind` and `All2AllIterative`. The difference between the two lies in the capability of handling blockage effects (see paragraph 2.2.1 on page 10).
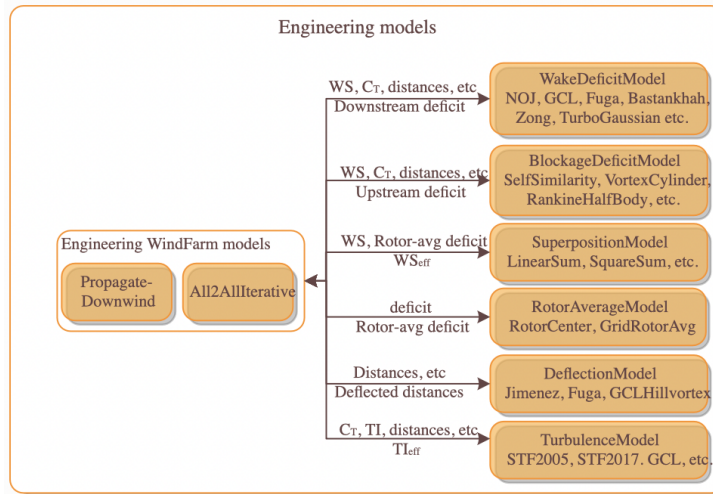
Figure 3.5: Architecture of Engineering Models. Figure from [15].

The main components constituting the `EngineeringWindFarmModel` are hereafter presented [15]:

- the **Wake Deficit Model** computes the reduction in wind speed, known as wake deficit, from one turbine to downstream turbines or sites within the wind farm (refer to 2.2 on page 8 and specifically to 2.2.2 on page 11 for further explanation).

- the **Blockage Deficit Model** computes the reduction in wind speed due to the induction region upstream the turbine.

- the **Superposition Model** defines the method by which deficits from multiple sources are aggregated.

- the **Rotor Average Model** determines how wind speeds reach the swept area of a turbine rotor and estimates the average wind speed over the rotor.

- the **Deflection Model** defines how wake deflection occurs due to factors such as yaw misalignment and sheared inflow, by adjusting the downwind and crosswind distances (refer to 2.2.3 on page 16).

- the **Turbulence Model** calculates the additional turbulence in the wake from one wind turbine to downstream wind turbines or sites within the wind farm.

- the **Ground Model** is employed to simulate the effects of the ground on inflow and wake characteristics.

Wake Deficit	Blockage Deficit	Superposition	Turbulence	Rotor Average	Deflection
NOJ	Fuga	Linear Sum	Steen Frandsen 2005	Rotor Center	Jimenez
Bastankhah Gaussian	Self Similarity Deficit	Squared Sum	Steen Frandsen 2017	Grid Rotor Average	Fuga
Zong Gaussian	Vortex Cylinder	Max Sum	GCL	Eq Grid Rotor Average	GCL Hill
Niayifar Gaussian	Vortex Dipole	Sqr Max Sum	Crespo Hernandez	GQ Grid Rotor Average	
Turbo Gaussian	Rankine Half Body	Weighted Sum		Polar Grid Rotor Average	
Turbo NOJ	Hybrid Induction			CGI Rotor Average	
Fuga	Rathmann				
Super Gaussian					
Carbajo Fuertes Gaussian					
GCL					

Table 3.3: Available models in PyWake. Table adapted from [15].

For what concerns Wake Deficit Models, the available Gaussian models are preferable to top-hat models, given that they can conserve deficit momentum (in isolation) and avoid singular behavior (step changes). The versions differ in their formulation of the streamwise wake expansion, which is governed by the initial wake diameter (at the wake origin) and its rate of expansion with downstream distance (see Figure 3.6) [15].
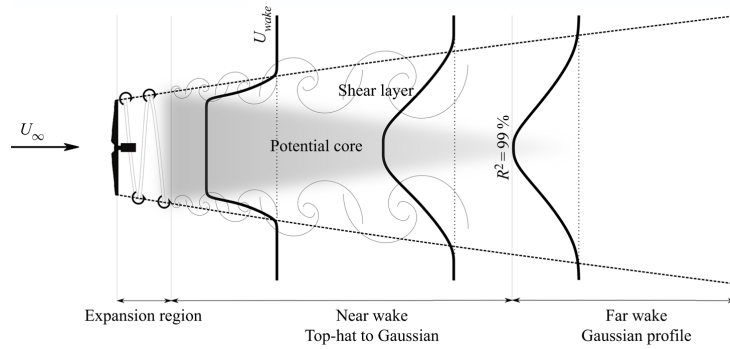
Figure 3.6: Schematic of the gradual growth of the mixing layer from the wake edge and the wake velocity distribution from the near wake (top-hat) to the far wake (self-similar Gaussian). Figure from [42].

4 | Methodology

This chapter is dedicated to outlining the procedural steps that culminate in the comparative analysis of control strategies discussed in Chapter 5. The necessary components for this foundational step include:

- Manipulating data obtained from the simulations executed using the turbine modeling tool;

- Implementing the selected derating algorithm;

- Integrating the "deratable" wind turbine into the wind farm modeling software.

The process is effectively illustrated in the flowchart seen in Fig. 4.1. This diagram highlights how the present methodology could be adapted for use with alternative tools beyond those applied in this study, for instance, `Cp-Lambda` and `FLORIS`.
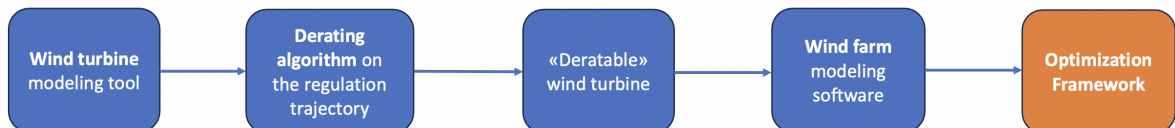
Figure 4.1: Flow diagram of the methodology followed within this thesis.

4.1. Wind turbine power curve optimization

Before illustrating how the derating strategy was implemented, it is important to define the domain in which the set of simulations on `HAWCStab2` were run and to give an overview on the resulting dataset.

The results were organized in an `xarray` Dataset with multiple dimensions and variables, outlined as follows:

Dimensions, setting the domain in which the simulations were run, are represented by:

- `wind_speed`: it ranges from 4 to 25 m/s and it has 22 discrete levels.

- `pitch`: it ranges from 0 to 50 degrees and it has 502 discrete levels.

- `rotor_speed`: it ranges from 6.0 to 8.68 revolutions per minute and it has 25 discrete levels.

Variables, constituting the performance data, are represented by:

- `V` $[\text{m} \cdot \text{s}^{-1}]$: Wind speed;

- `P` $[\text{kW}]$: Aerodynamic power;

- `T` $[\text{kN}]$: Aerodynamic thrust;

- `C_P` $[-]$: Power coefficient;

- `C_T` $[-]$: Thrust coefficient;

- `Pitch Q` $[\text{N} \cdot \text{m}]$: Pitch torque;

- `Flap M` $[\text{kN} \cdot \text{m}]$: Hub root out-of-plane bending moment;

- `Edge M` $[\text{kN} \cdot \text{m}]$: Hub root in-plane bending moment;

- `Pitch` $[\text{deg}]$: blade pitch angle;

- `Speed` $[\text{rpm}]$: rotor speed;

- `Tip x` $[\text{m}]$: In-plane tip position relative to the rotor center;

- `Tip y` $[\text{m}]$: Out-of-plane tip position relative to the rotor center;

- `Tip z` $[\text{m}]$: Radial tip position relative to the rotor center;

- `J_rot` $[\text{kg} \cdot \text{m}^2]$: Rotor inertia;

- `J_DT` $[\text{kg} \cdot \text{m}^2]$: Inertia of entire drivetrain including rotor;

- `Tors.` $[\text{rad}]$: Torsional component of chord rotation (here torsional refers to rotation about the spanwise unit-vector of the chord coordinate system of the undeformed blade;

- `Torque` $[\text{kN} \cdot \text{m}]$: Torque.

The first step involved the writing of a Python routine to define the power curve of the reference turbine by implementing the algorithm below, for each wind speed:

$$\omega, \beta = \underset{\omega, \beta}{\arg\max} \, P(\omega, \beta)$$

$$\text{Subject to:} \begin{cases} 0 \le T(\omega, \beta) \le T_r \\ \omega_{\min} \le \omega \le \omega_{\max} \\ \beta_{\min} \le \beta \le \beta_{\max} \end{cases}$$

where ω represents the rotor speed, β the pitch angle, P the power and T the torque, with T_r equal to 11.740 MNm (see Table 3.1 on page 23). Utilizing specialized libraries for numerical analysis and visualization, i.a. Scipy, the for loop in the script iterated over the specified range of wind speeds. For each wind speed within this range, it performed an optimization process using Sequential Least Squares Programming (SLSQP) method to find the optimal pitch angle and rotor speed that would maximize the power output of the wind turbine. This was achieved by minimizing the negative of the power output, using constraints to ensure the operational limits were not exceeded. The results of this optimization, including the optimal parameters and their corresponding power outputs, were then compiled into an array for further analysis and visualization. The result of this operation can be seen in Table 4.1, where only blade pitch, rotor speed and power are highlighted, and in the set of graphs that display the trend of the main performance parameters against wind speed (Fig. 4.2). As noticeable, the plots and the values in the table correspond to those presented in the Technical Report (Fig. 3.2 on page 24 and Table 3.2 on page 25) confirming the validity of the routine.

| Wind speed [m/s]	Pitch [deg]	Rotor speed [rpm]	Aerodynamic power [kW]
4.00	2.487	6.00	457.7
5.00	1.251	6.00	1096.9
6.00	0.000	6.00	2003.1
7.00	0.000	6.77	3183.6
8.00	0.000	7.75	4734.6
9.00	0.000	8.68	6696.5
10.00	0.000	8.68	8991.5
11.00	2.379	8.68	10638.6
12.00	5.879	8.68	10638.6
13.00	8.200	8.68	10638.6
14.00	10.099	8.68	10638.6
15.00	11.769	8.68	10638.6
16.00	13.292	8.68	10638.6
18.00	16.056	8.68	10638.6
20.00	18.569	8.68	10638.6
25.00	24.185	8.68	10638.6

Table 4.1: Regulation trajectory.
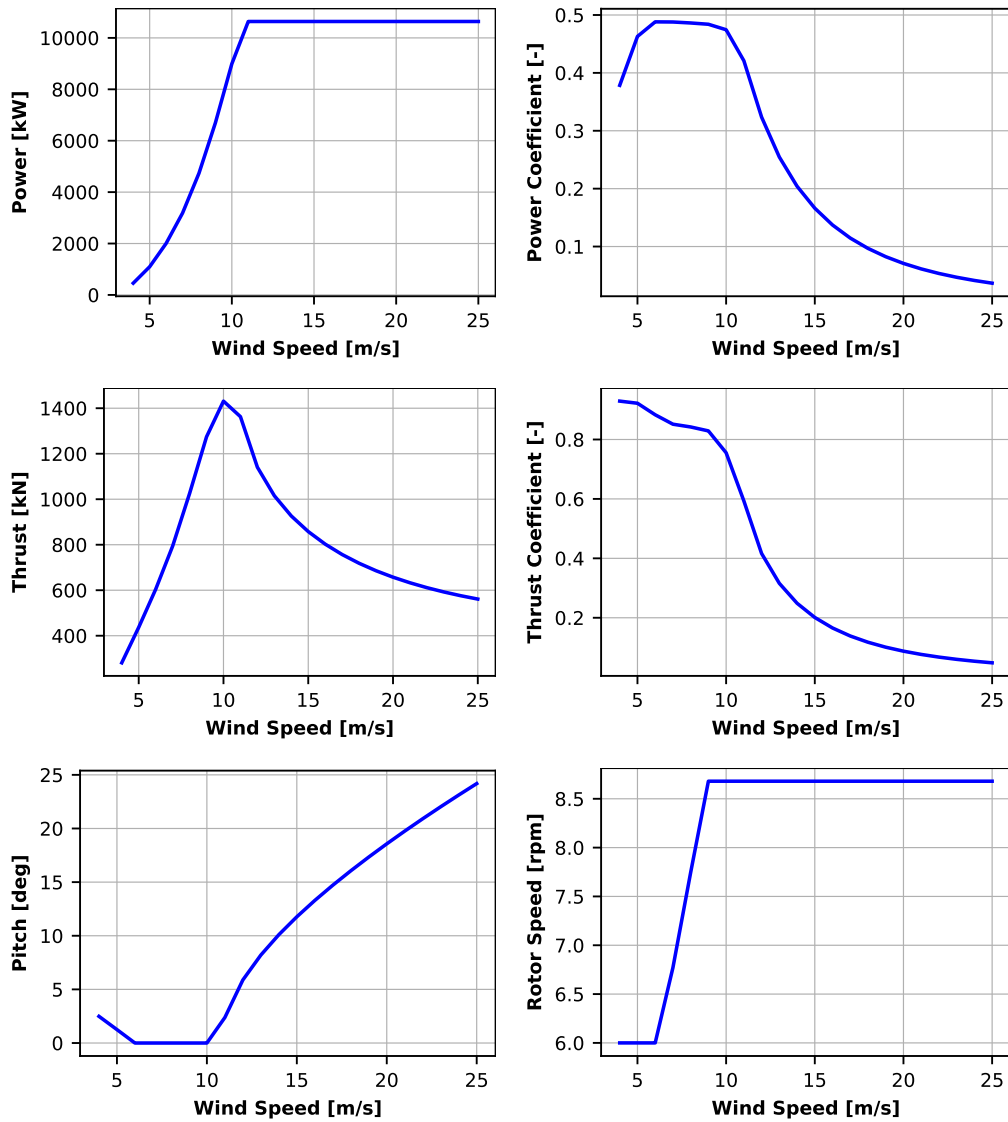
Figure 4.2: Steady-state performance and operation of the 10-MW rotor.

4.2. Implementation of the derating algorithm

Among the different kinds of down-regulation strategies (refer to [30] for further knowledge), the algorithm proposed by Meng et al. was chosen to tackle the issue of power optimization within a wind farm [33].

The aim of the minimum C_T control strategy is therefore twofold [33]:

- by reducing wake effects and increased turbulence, it offers the advantage of lessening fatigue loads across the wind farm;

- despite a decrease in the power output of individual turbines undergoing derating, it can enhance the overall power generation of the wind farm.

The optimization problem, for a given derating percentage ΔP, consists in determining the optimal rotor speed, ω, and pitch angle, β, such that the minimization of C_T is satisfied:

$$\omega_d, \beta_d = \arg \min_{\omega, \beta} C_T(\omega, \beta)$$

$$\text{Subject to:} \begin{cases} C_{P,d}(\omega_d, \beta_d) = (100 - \Delta P)C_{P,\max} \\ \omega_{\min} \leq \omega_d \leq \omega_{\max} \\ \beta_{\min} \leq \beta_d \leq \beta_{\max} \end{cases}$$

with the subscript d standing for the derated operation. In the specific case of the study presented in [33], the selected reference turbine was a DTU 10-MW model whose power and thrust coefficients were plotted as a function of λ and β in the following contour plot (Fig. 4.3):
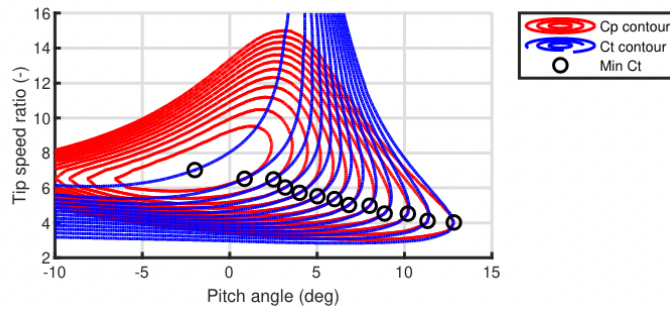
Figure 4.3: C_P, C_T contours and minimum C_T operational points. Figure from [33].

Implementing the above algorithm on Python using the optimization method of Sequential Least Squares Programming (SLSQP) within the `SciPy.optimize.minimize` function for the IEA 10-MW reference turbine did not result in the first place in a successful outcome,

calling for a deeper analysis to identify the issue. To ease the optimization process, a graphical method was therefore adopted to find the value pair (ω, β)[1] that ensures the minimum C_T operational points for each wind speed, similarly to Fig. 4.3. The contour plots that were generated displayed an issue related to the fact that the isolines of C_P and C_T were almost parallel, as depicted in Fig. 4.4 for the case at wind speed = 18 m/s.
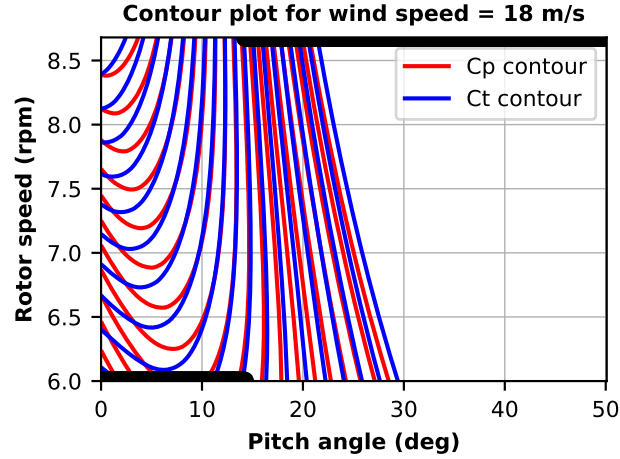

Figure 4.4: C_P, C_T contours for wind speed = 18 m/s.

The issue of parallel isolines for C_T and C_P refers to the problem of collinearity in mathematical and statistical models. Collinearity occurs when two or more predictor variables in a regression model are highly linearly correlated, making it difficult to discern the independent effect of each predictor on the outcome variable.

In the context of the present optimization, parallel isolines for C_T and C_P indicate a similar challenge:

1. **Indeterminacy:** Just as collinearity obscures the unique contribution of each predictor to the response variable, parallel isolines of C_T and C_P complicate the optimization process by indicating a non-unique influence of operational parameters (like blade pitch angle and rotor speed) on these coefficients.

2. **Infinite Solutions:** Severe collinearity in regression analysis can lead to an infinite number of solutions for the model's coefficients. Similarly, the parallelism of C_T and C_P isolines suggests an infinite array of operational parameter settings that yield the same C_T and C_P values, making it difficult to pinpoint a singular optimal solution.

3. **Sensitivity:** Models with collinear variables are sensitive to minor data changes,

---

[1]The choice of using the rotor speed ω instead of the tip-speed ratio λ does not hinder the analysis.

affecting the stability and reliability of coefficient estimates. Analogously, when C_T and C_P isolines are parallel, minor adjustments in operational parameters may lead to significant and potentially unstable variations in performance outcomes.

One of the suggested ways to address collinearity in literature is to introduce additional constraints. This was done by[2]:

- fixing the rotor speed ω to the optimal value $\omega_{P,\max}$ provided by the power maximization process in 2.3.1, for each wind speed;

- keeping the pitch β as the only design variable.

The algorithm was therefore adjusted to better suit the specificity of this thesis as follows:

$$\beta_d = \arg\min_{\beta} C_T(\beta)$$

$$\text{Subject to:} \begin{cases} C_{P,d}(\beta_d) = \Delta P C_{P,\max} \\ \omega_d = \omega_{P,\max} \\ \beta_{\min} \leq \beta_d \leq \beta_{\max} \end{cases}$$

valid for each wind speed between cut-in and cut-out.

Taking into account an array of deratings ranging from 0% to 100%, where 0% corresponds to the nominal power curve and 100% to fully derated operation, four plots were obtained (see Fig. 4.5). As noticeable, the trends match those shown in the set of graphs in Fig. 4.2, proving the reliability of the adopted algorithm.

---

[2]Choosing the rotor speed as the only design variable, instead, would have led to a slower torque control because of the rotor inertia.

4.3.   Integration of the derating strategy within Py-Wake

Once the implementation of the chosen derating strategy was proven to be valid, the challenge transitioned to the integration of this derating capability within the `PyWake` framework, a tool renowned for its modular architecture — a feature that significantly contributes to its versatility and adaptability. The core challenge involved identifying the methodological approach to tailor `PyWake`'s built-in functionalities to accurately represent a turbine with derating capabilities. This adaptation process is pivotal in enabling the precise characterization of a "deratable" turbine within the `PyWake` environment, thereby enhancing the tool's utility in wind turbine optimization scenarios.

To do so, the initial step entailed the collection of the optimization outcomes of thrust coefficient C_T and power output P from section 4.2 into two distinct arrays. The arrays are displayed in Table 4.2 to facilitate a comprehensive understanding of the numerical data underpinning the optimization process.

To enhance the dataset's granularity for `PyWake`, it became evident that the optimization process delineated in section 4.2 required modification. Specifically, the derating array's step size was reduced to 1% from the initial 10%. This adjustment was critical to ensuring a more refined analysis when utilizing `OpenMDAO` for subsequent evaluations, thereby facilitating smoother execution of the analytical processes.

The writing of the code is subdivided into two parts: the definition of the turbine and the wind farm simulation setup and visualization.

4.3.1.   Definition of the IEA-10 MW derated turbine

The procedure started with the establishment of an array representing a range of wind speeds, extending from 4 m/s to 25 m/s. An extra wind speed value (4.0 + 1e-8) was added to avoid a vertical slope from the turbine's cut-in wind speed, ensuring a smooth transition in the power curve. Following this, the arrays of power and C_T values were loaded and adjusted by an electromechanical efficiency factor to account for electrical system losses. Subsequently, the initialization of a `PowerCtFunctionList` object was carried out[3]. This object was populated with `PowerCtTabular` instances, each representing a distinct derating level, which are in turn based on the mapped derated power and C_T arrays

---

[3]`WindTurbines` can be defined using a `PowerCtFunctionList` in order to achieve having a "mode" that differentiates the turbines. In this case, the mode is the derating, and each turbine derated by a different factor corresponds to a `PowerCtTabular` instance.
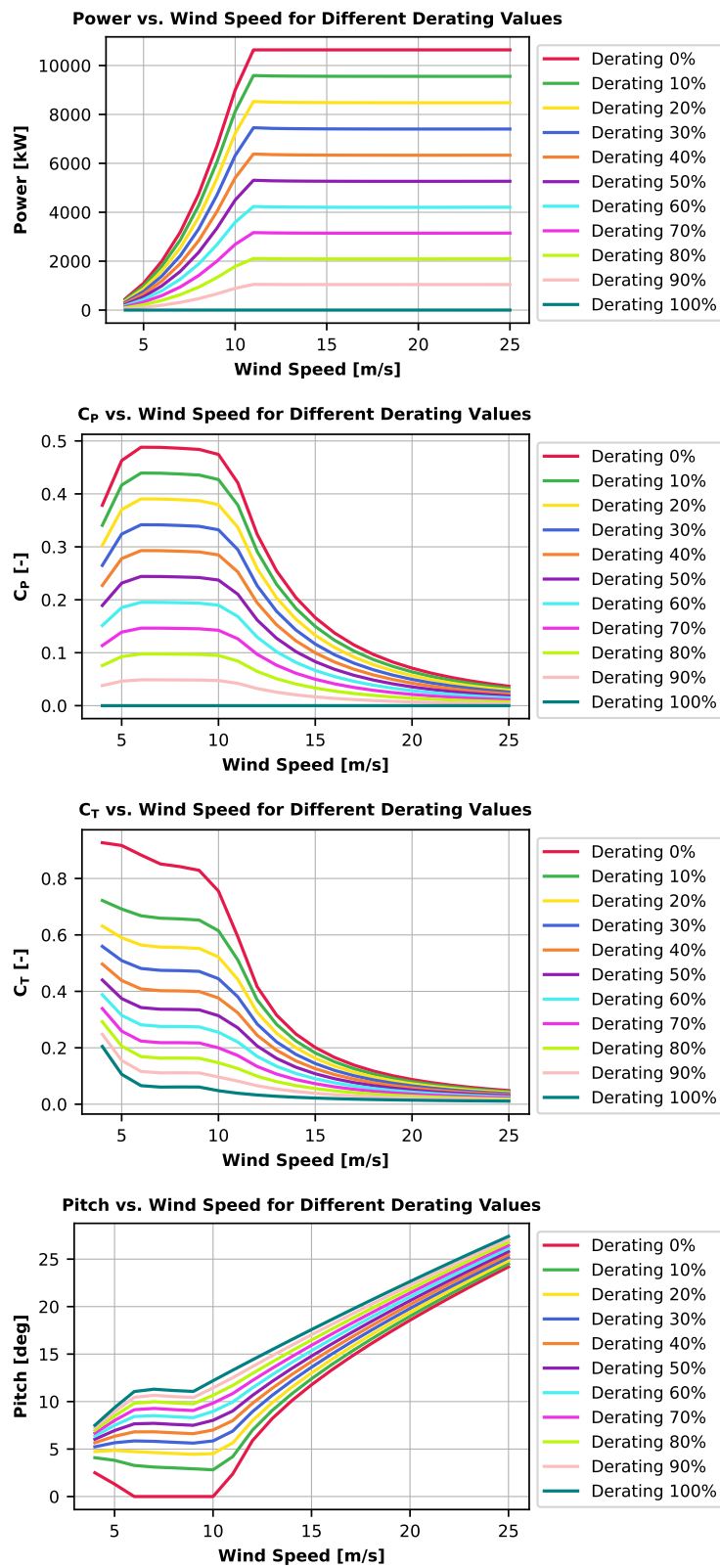
Figure 4.5: Trend of P, C_P, C_T, β for different derating percentages.

Wind speed [m/s]	0% derating		20% derating		40% derating		60% derating		80% derating		100% derating	
	Power [kW]	C_T [-]	Power [kW]	C_T [-]	Power [kW]	C_T [-]	Power [kW]	C_T [-]	Power [kW]	C_T [-]	Power [kW]	C_T [-]
4.0	457.675	0.927	365.062	0.632	273.401	0.497	182.047	0.388	90.923	0.292	-0.000	0.205
5.0	1096.845	0.917	873.818	0.590	653.833	0.439	434.988	0.315	217.073	0.206	0.001	0.106
6.0	2003.082	0.883	1595.393	0.564	1192.858	0.409	792.926	0.281	395.338	0.169	-0.001	0.066
7.0	3183.578	0.851	2538.692	0.557	1897.823	0.402	1260.906	0.276	628.243	0.163	-0.001	0.061
8.0	4734.399	0.842	3784.304	0.555	2829.737	0.402	1879.620	0.275	936.018	0.164	0.006	0.061
9.0	6696.478	0.829	5369.404	0.552	4017.756	0.400	2668.642	0.274	1328.322	0.163	0.001	0.061
10.0	8991.501	0.755	7223.008	0.522	5407.373	0.376	3590.394	0.255	1785.591	0.147	-0.008	0.048
11.0	10638.556	0.593	8528.064	0.442	6382.881	0.324	4236.757	0.220	2105.997	0.126	-0.010	0.039
12.0	10638.557	0.416	8502.547	0.326	6357.253	0.245	4218.685	0.170	2097.307	0.099	0.001	0.033
13.0	10638.545	0.316	8492.552	0.252	6346.517	0.191	4211.088	0.134	2093.816	0.080	0.008	0.028
14.0	10638.549	0.249	8486.998	0.200	6340.512	0.154	4206.910	0.109	2092.078	0.066	0.007	0.025
15.0	10638.552	0.201	8483.528	0.163	6336.837	0.126	4204.499	0.090	2091.152	0.056	-0.006	0.022
16.0	10638.554	0.166	8481.190	0.135	6334.497	0.105	4203.108	0.076	2090.713	0.047	0.006	0.020
17.0	10638.545	0.139	8479.682	0.113	6333.025	0.089	4202.339	0.065	2090.636	0.041	-0.012	0.018
18.0	10638.551	0.118	8478.732	0.097	6332.102	0.076	4202.012	0.056	2090.714	0.036	-0.007	0.017
19.0	10638.537	0.101	8478.108	0.083	6331.746	0.066	4202.002	0.049	2090.964	0.032	-0.001	0.015
20.0	10638.550	0.088	8477.781	0.073	6331.652	0.058	4202.234	0.043	2091.319	0.029	-0.009	0.014
21.0	10638.559	0.077	8477.571	0.064	6331.667	0.051	4202.611	0.038	2091.720	0.026	0.080	0.013
22.0	10638.467	0.068	8477.529	0.056	6331.909	0.045	4203.113	0.034	2092.189	0.023	-0.021	0.013
23.0	10638.564	0.060	8477.619	0.050	6332.259	0.041	4203.708	0.031	2092.708	0.021	0.010	0.012
24.0	10638.596	0.054	8477.833	0.045	6332.807	0.037	4204.420	0.028	2093.299	0.020	0.048	0.011
25.0	10638.602	0.048	8478.169	0.041	6333.446	0.033	4205.192	0.026	2093.998	0.018	0.092	0.011

Table 4.2: Power and C_T arrays for different derating percentages.

to the defined wind speed array. This setup allows the turbine model to accurately select the appropriate power and C_T curve based on the derating level specified for any given simulation. Finally, a `WindTurbineobject`, named `iea10mw_derated`, was instantiated. This step involved specifying the turbine's name, diameter, hub height, and attaching the `powerCtFunction` as the newly defined `PowerCtFunctionList`.

This procedure yielded plots similar to those previously obtained, with the notable distinction being a more gradual onset evident in the graph, as illustrated in Fig. 4.6.
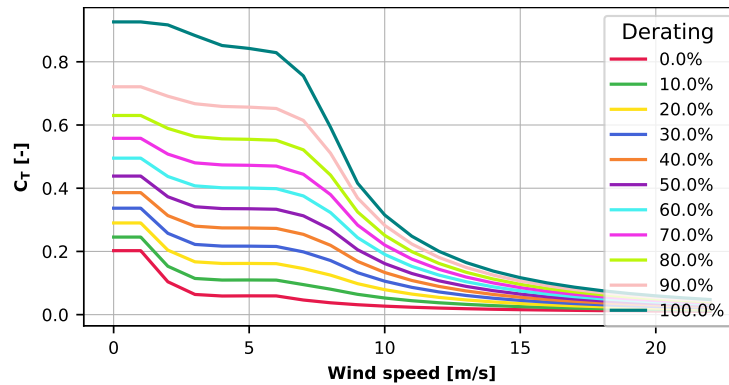
Figure 4.6: C_T as a function of the wind speed.

4.3.2. Site definition

`PyWake` contains a few predefined sites of different complexities, among which `Hornsrev1` was selected. Horns Rev 1 is an offshore wind farm that set a remarkable precedent in the wind energy sector. Located off the west coast of Denmark's Jutland peninsula, Horns Rev 1 was a groundbreaking project inaugurated in 2003, becoming the world's first large-scale offshore wind farm. With 80 Vestas V80 turbines, each having a capacity of 2 MW, the farm covers an area of 20 km² and paved the way for an industry that 20 years later relies on 60 GW of offshore wind capacity installed across 19 countries, around 400 times the Horns Rev 1 capacity. The technological hurdles faced in developing this wind farm gave birth to many pioneering solutions that are today industry standard, proving the feasibility and reliability of offshore wind energy on a grand scale and highlighting the enduring legacy of this landmark project in advancing sustainable energy solutions.

Figure 4.7: Photograph of the Horns Rev 1 offshore wind farm 12 February 2008 at around 10:10 UTC seen from the southeast. Taken from [20].

`Hornsrev1` provides default settings which can be overwritten according to the specific needs. In the present study, they were adjusted as follows:

- the wind direction was put equivalent to the default property `site.default_wd`, with a range 0-360° in bins of 1°;

- the wind speed was changed to 4-25 m/s (being them the cut-in and cut-out speeds of the reference turbine) with respect to the default property `site.default_ws`, having instead a range of 3-25 m/s in bins of 1 m/s;

- the wind turbine positions were modified according to the investigated layout, as opposed to the original layout `site.initial_position.T` that features 80 turbines placed in a parallelogram geometry as shown in Fig. 4.8.
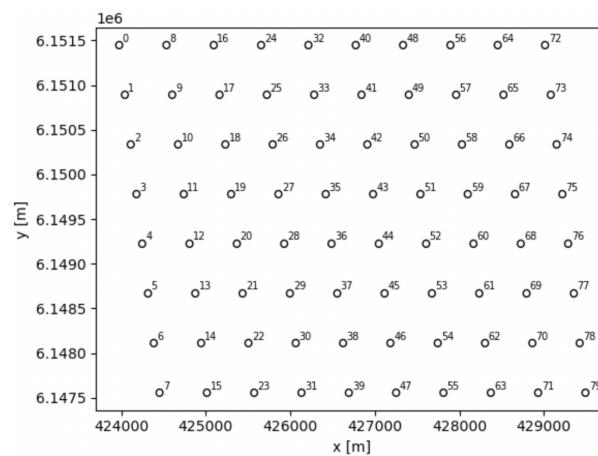
Figure 4.8: Default geometry for Horns Rev 1 wind farm. Taken from [15].

Among the following three `Site` classes PyWake employs:

- `XRSite`

- `UniformWeibullSite`

- `WaspGridSite`

`Hornsrev1` is based on `UniformWeibullSite`, meaning that it is characterized by a Weibull distributed wind speed, a predefined wind sector probability and uniform wind over a flat wind area. The Weibull distribution and the wind rose, which visually depict these characteristics, are presented in Figure 4.9 and Figure 4.10, respectively.
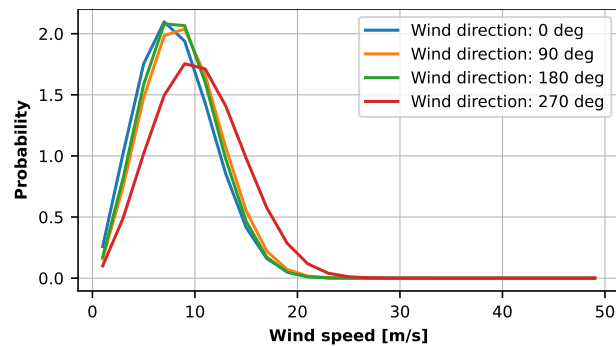
Figure 4.9: Weibull distribution.
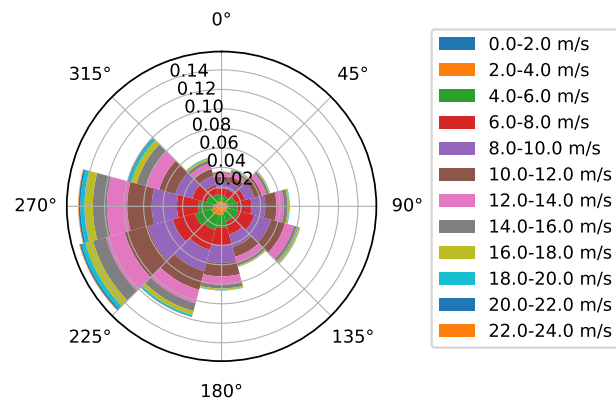
Figure 4.10: Wind rose.

4.3.3.   Wind farm definition

Among the models discussed in Section 3.3.1, the `Zong_PorteAgel_2020` model, referred to in Table 3.3 as the Zong Gaussian model, was selected for its distinctive characteristics. This model includes the laws of mass and momentum conservation and features a Gaussian wake profile, as illustrated in Fig. 3.6. It is worth to highlight that Zong and Porté-Agel

[44] enhanced a previously established model from 2016 [34] by incorporating modified elements of the Shapiro wake model [39]. These modifications include the phased increase of the thrust force, culminating in the full thrust effect at a distance of 2D downstream from the turbine, and maintaining an expansion factor that does not diminish below the rotor's diameter.

The model requires specific input parameters, namely the `iea10mw_derated` as the `WindTurbines` object and `Hornsrev1` as the `Site` object. Additionally, the precise locations of the turbines are delineated through the specification of their x and y coordinates, thereby establishing a particular layout that can be adjusted as needed. A critical component of this model is the provision of an array containing the derating factors for each turbine within the specified layout. This array plays a pivotal role in generating simulation results, which are further leveraged to develop both flow and Annual Energy Production (AEP) maps.

This methodological approach not only enables a comprehensive evaluation of the wind farm's projected performance but also serves as an essential phase in the refinement of the wind farm's control strategy, aiming at maximizing efficiency and output.
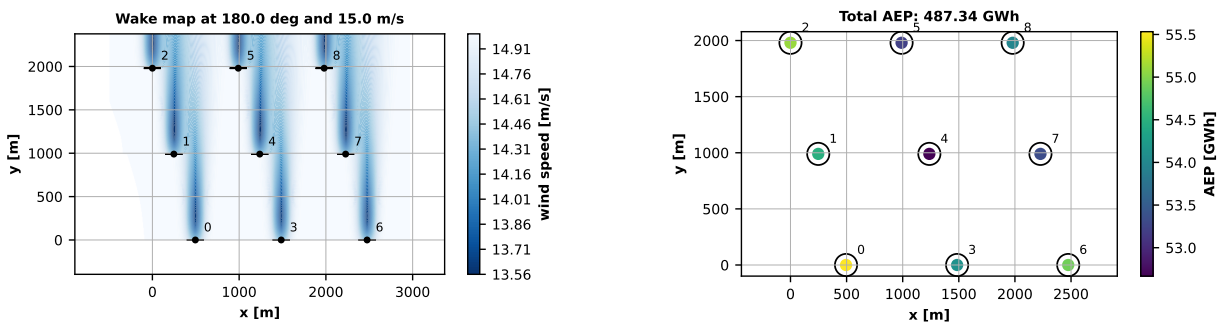
Figure 4.11: Examples of a flow map and an AEP map for a wind farm characterized by `iea10mw_derated` turbines with no derating applied, placed in a parallelogram layout.

5 | Simulations and results

This chapter consolidates and interprets all findings to date within an optimization framework, whose aim is to maximize the wind farm's power output. This is achieved by analyzing how derating and yaw-based wake redirection control strategies affect a variety of cases, by means of an open-loop approach. A key tool in this process is `OpenMDAO`, a multidisciplinary optimization framework designed by NASA to facilitate solving complex engineering design problems, involving multiple disciplines and interacting subsystems.

`OpenMDAO`'s key features include:

- Modular architecture, that allows for easy integration of tools from different disciplines;

- Gradient-based optimization, which supports efficient sensitivity analysis and gradient-based optimization methods;

- Component-based design, that facilitates the reuse of models and analyses;

- Python-based, making it accessible to a wide range of users and allowing for easy integration with other Python libraries and tools.

5.1. Definition of the components

The core advantage of `OpenMDAO` lies in its component-based architecture, a pivotal aspect leveraged throughout this thesis. It facilitated the creation of versatile components tailored to specific input parameters like yaw and derating, all while preserving a consistent structural framework. More precisely, the component that was developed belongs to `OpenMDAO`'s `ExplicitComponent` class[1] in which various options, inputs and output were defined so as to arrange in a structured code the different elements that customize and characterize a wind farm. The options include wind speed, wind direction and wind turbines location, while inputs refer to yaw and derating for each turbine. Finally, a

---

[1]In `OpenMDAO`, explicit variables are defined by writing a class that inherits from the `ExplicitComponent` class. The explicit variables would be considered outputs while the variables on which they depend would be considered inputs [41].

compute function allows to calculate the output in terms of total power, which eventually represents the objective with respect to which the `OpenMDAO` problem will be optimized. In terms of optimizer, COBYLA (Constrained Optimization by Linear Approximation) was chosen for its possibility to support constraints, but differently from SLSQP it is derivative-free.

5.2.   Sanity check with two turbines

A basic two-turbine configuration was chosen as the wind farm layout. While this layout is simple and understandably fails to capture the complex dynamics found in an actual wind farm with multiple turbines, it should be considered as a foundational step. This initial framework sets the stage for the creation of a more detailed model that could be further investigated in future research.

The turbines are placed at the same y coordinate and spaced along the x-axis by a varying multiple of the rotor's diameter, as shown in Fig. 5.1.
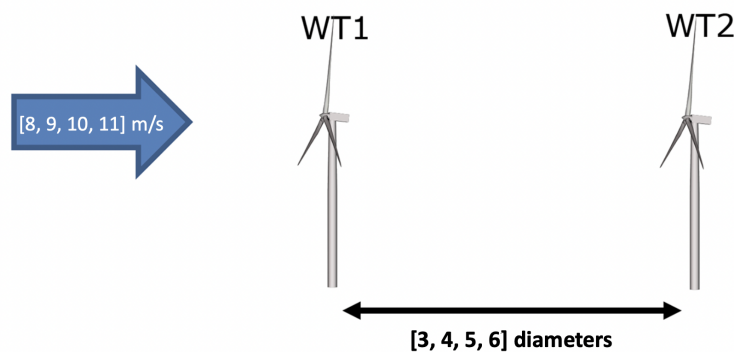
Figure 5.1: Wind farm layout. Figure adapted from [36]

For each control strategy, the optimization process involves the testing of the wind farm performance by varying:

1. the wind speed in [8, 9, 10, 11] m/s;

2. the wind direction in [0, 90, 180, 270] degrees;

3. the spacing in [3, 4, 5, 6] rotor's diameter.

5.2.1. Baseline case

When no control strategy is adopted, the power losses due to the wake effect become evident. In order to grasp such difference, the values of power output at 90 and 270 degrees of wind direction are reported in Table 5.1. As a matter of fact, given the chosen layout, these are the only wind directions that raise an aerodynamic interaction, while 0 and 180 degrees are not of interest for the comparison across control strategies.

Wind speed = 8 m/s	
Spacing	Power [kW]
3D	5156.8
4D	5547.6
5D	6039.3
6D	6433.2

Wind speed = 9 m/s	
Spacing	Power [kW]
3D	7438.3
4D	8045.1
5D	8672.6
6D	9227.1

Wind speed = 10 m/s	
Spacing	Power [kW]
3D	10743.1
4D	11493.5
5D	12308.8
6D	12977.6

Wind speed = 11 m/s	
Spacing	Power [kW]
3D	14782.2
4D	15722.5
5D	16528.6
6D	17268.6

Table 5.1: Wind speed versus power output for various spacings.

5.2.2. Derating only

The first control strategy involves the exclusive application of derating. As easily fore-seeable, the problem shows to be symmetrical for the wind direction pairs 0-180 degrees (North-South) and 90-270 degrees (East-West).

0-180°

The following considerations apply:

- Changing the diameter does not influence the power output of the two turbines;

- No derating is applied, because the turbines are not aerodynamically interfering with one another;

- Of course, higher wind speeds correspond to larger values of total power output, as reported in Table 5.2.

Wind speed [m/s]	Total power [kW]
8.0	9038.0
9.0	12783.6
10.0	17164.8
11.0	20309.0

Table 5.2: Wind speed and corresponding total power output, for a two-turbine layout and wind directions equal to 0 and 180 degrees.

90-270°

Based on the outcomes of the simulations, several key considerations have been identified. They include:

- Changing the diameter does affect the power output, given that the optimization results in a specific derating value. It is noticeable that the further apart the turbines are placed, the less derating is applied because of wake recovery;

- As the wind speed increases, down-regulation is not of help, meaning that the increase in power output of the downwind turbine doesn't offset the curtailment applied on the upstream one.

Because the results of the simulations are independent of the direction, as 90 and 270 degrees represent a mirrored condition[2], the derating of the upstream turbine[3] is reported in Table 5.3, together with the resulting power output sum, as the spacing varies for all wind speeds in [8, 9 , 10, 11] m/s.

---

[2]This is valid because the analysis focuses on power. Should the AEP be examined instead, the symmetry would cease to exist.

[3]Obtained as an average of the two derating percentages, whose variation is related to a natural oscillation of the decimal digits.

Wind speed = 8 m/s		
Spacing	Derating of the upstream turbine [%]	Power [kW]
3D	12.7	5596.3
4D	14.3	5965.8
5D	9.8	6355.6
6D	7.3	6696.8

Wind speed = 9 m/s		
Spacing	Derating of the upstream turbine [%]	Power [kW]
3D	13.8	7994.4
4D	9.4	8506.7
5D	10.1	9015.9
6D	7.3	9507.4

Wind speed = 10 m/s		
Spacing	Derating of the upstream turbine [%]	Power [kW]
3D	12.5	11092.9
4D	7.8	11797.3
5D	5.5	12465.7
6D	5.5	13103.5

Wind speed = 11 m/s		
Spacing	Derating of the upstream turbine [%]	Power [kW]
3D	3.1	14804.2
4D	0.0	15722.5
5D	0.0	16528.6
6D	0.0	17268.6

Table 5.3: Derating and power values for 90-270 degrees of wind direction, as spacing and wind speed vary.

For the sake of completeness, an additional simulation was conducted at a wind speed of 12 m/s to demonstrate that, when surpassing the rated wind speed of 11 m/s, the upstream turbine does not necessitate derating, even with a spacing of three rotor diameters.

Wind speed $= 12\,\mathrm{m/s}$		
Spacing	Derating of the upstream turbine [%]	Power [kW]
3D	0.0	18575.7
4D	0.0	19152.1
5D	0.0	19610.0
6D	0.0	19975.9

Table 5.4: Derating and power values for 90-270 degrees of wind direction, as spacing varies.

Additionally, a graphical method was employed to further validate the optimization results. By setting the wind direction at 270°, wind turbine 1 is identified as the upstream turbine. Adjusting its derating leads to a decrease in its power output, while simultaneously increasing the power output of wind turbine 2. The graph illustrating this dynamic (Fig. 5.2) shows that, with a wind speed of 10 m/s and a spacing of four diameters, the optimal combined power output of 11797.34 kW for both turbines is achieved at an 8% derating level, aligning precisely with the results presented in Table 5.3.
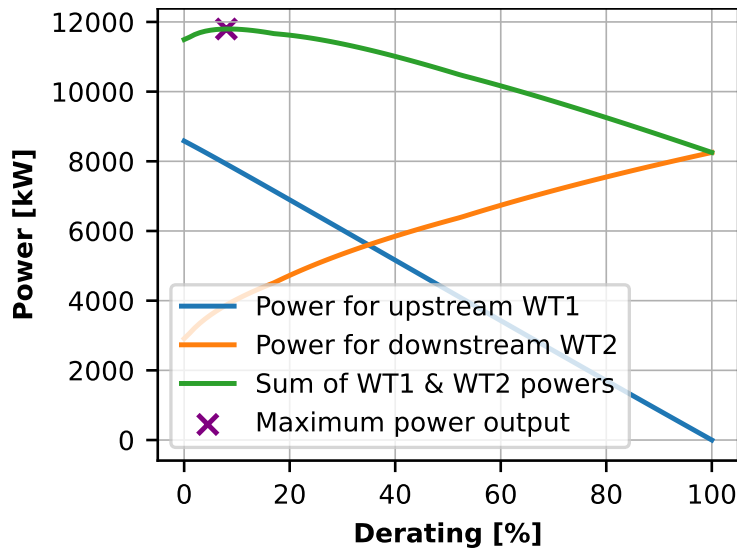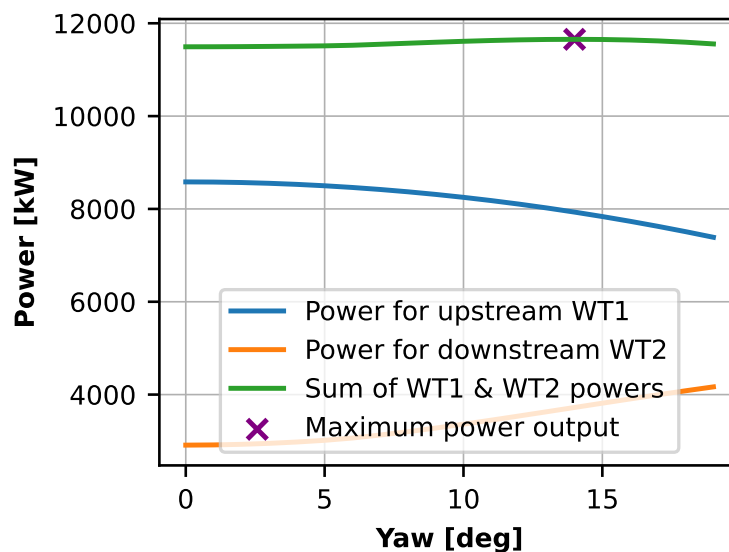

Figure 5.2: Graphical method showing the trend of individual and collective power output with respect to the derating percentage of the upstream turbine, at wind speed equal to 10 m/s and spacing equal to 4 rotor diameters.

5.2.3. Wake redirection only

The second strategy implemented was wake redirection, incorporating the `OpenMDAO` component with additional inputs for turbine 1 and 2's yaw misalignment. The wind farm

model (see Section 3.3 on page 26) was enhanced with two options: the deflection and superposition models. The Jimenéz (see Section 2.2.3 on page 16) wake deflection model was selected for the former, and the Max Sum approach for the latter. With respect to the previous optimization problem, the derating percentage was constrained to 0% and the lower and upper boundaries for the yaw angle were set to 0 and 20 degrees, respectively.

Just like Section 5.2.2, it is possible to subdivide the simulations according to the wind directions pairs 0-180° and 90-270°.

0-180°

The turbines are facing either North or South and no wake redirection is applied. The spacing between the turbines does not affect their total power output, and the whole problem collapses to the power output variation being function of the wind speed only, as shown in Table 5.2.
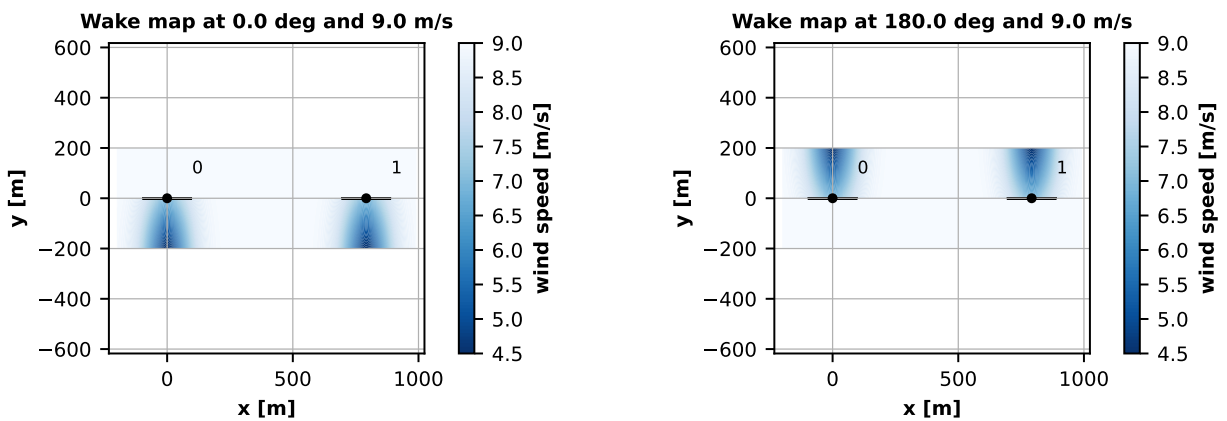
Figure 5.3: Wake maps at 0° (left) and 180° (right), with a 4D spacing.

90-270°

This set of simulations has produced the results reported in Table 5.5 and leads to the following observations:

- The yaw angle does not exhibit a consistent increasing pattern with reduced spacing between turbines. However, the observed values are justifiable considering that a 3D spacing is within the near-wake region, while a 6D spacing is quite conservative for this type of analysis. Notably, there is a reduction of 2 degrees in the yaw angle when the spacing changes from 4D to 5D, spacings which are typically used in practice;

- Like in the derating case, as wind speeds rise, the effectiveness of wake redirection

for mitigating wake-induced losses decreases. This is because the advantage gained by the downwind turbine does not sufficiently compensate for the performance loss of the upwind turbine, resulting in a net negative outcome.

Wind speed = 8 m/s		
Spacing	Yaw angle of the upstream turbine [degrees]	Power [kW]
3D	18.2	5386.6
4D	19.3	5898.9
5D	17.5	6374.9
6D	15.8	6730.0

Wind speed = 9 m/s		
Spacing	Yaw angle of the upstream turbine [degrees]	Power [kW]
3D	14.9	7674.6
4D	16.6	8412.1
5D	17.5	9038.9
6D	15.7	9555.0

Wind speed = 10 m/s		
Spacing	Yaw angle of the upstream turbine [degrees]	Power [kW]
3D	9.9	10783.8
4D	14.0	11654.3
5D	12.1	12428.3
6D	13.2	13120.5

Wind speed = 11 m/s		
Spacing	Yaw angle of the upstream turbine [degrees]	Power [kW]
3D	0.0	14782.2
4D	0.0	15722.5
5D	0.0	16528.6
6D	0.0	17268.6

Table 5.5: Yaw angle and power values for 90-270 degrees of wind direction, as spacing and wind speed vary.

Just like in Section 5.2.2, a graphical approach was also adopted here to assess the accuracy of the optimization outcomes. Using the identical benchmark scenario (with wind direction at 270°, wind velocity at 10 m/s, and a separation distance of 4D), the curve
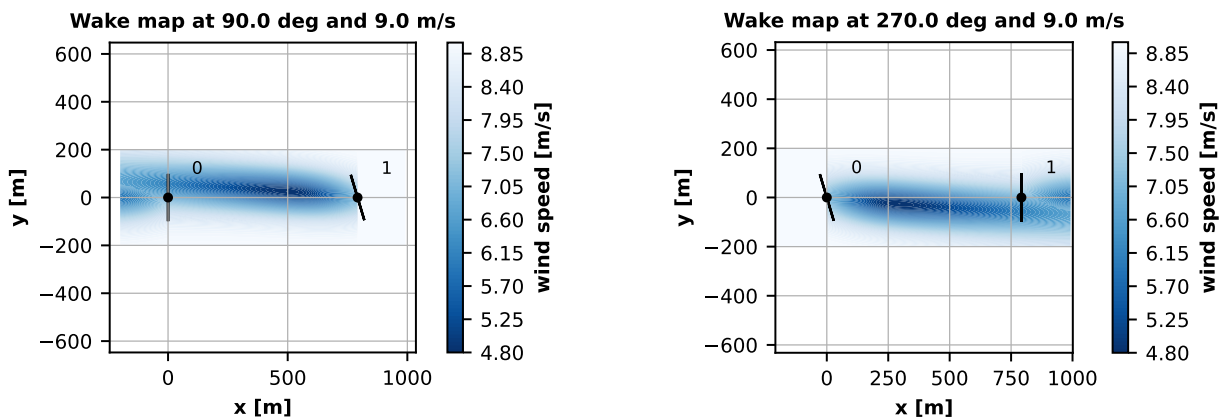
Figure 5.4: Wake maps at 90° (left) and 270° (right) at 9 m/s, with a 4D spacing. The upstream turbine is yawed by 16.6 degrees.

patterns distinctly illustrate that as the yaw angle of the turbine positioned upstream is increased, its power output decreases, whereas the power generated by the downstream turbine rises. The optimal balance is attained at a 14° yaw misalignment, which matches the figure listed in Table 5.5.

Figure 5.5: Graphical method showing the trend of individual and collective power output with respect to the yaw misalignment of the upstream turbine, at wind speed equal to 10 m/s and spacing equal to 4 rotor diameters.

5.2.4. Combination of WR and AIC

Using wake steering and derating strategies aimed solely at maximizing power has turned out to be a problem with numerical instability. When analyzed, the simulations presented

varying yaw and derating configurations for wind directions of 90° and 270°, despite the expectation of identical outcomes due to the mirror symmetry of the scenarios. This situation indicated the presence of local minima and the difficulty to identify a global optimum due to `OpenMDAO`'s reliance on gradient-based optimization and the inherent fragility of formulating the problem in such a manner. In recent years many techniques have been suggested for the avoidance of local optima, among which the multi-start method stands out for its simplicity. It consists in re-starting the search of the solution once a region has been extensively explored, which, in the case of this thesis, translated in feeding into the `OpenMDAO`'s problem different initial guesses of yaw misalignment and derating percentage for the upstream turbine.

In practice, considering a benchmark case at 10 m/s of wind speed and 90° of wind direction, with turbines spaced by [3,4,5,6] rotor diameters, the multi-start method delivered the results shown in Table 5.6.

In terms of power output, the solutions do not differ significantly, while they differ substantially in the combination of the optimal yaw and derating.

Consequently, a parametric analysis was conducted to pinpoint the region of combinations of yaw angle and derating for the upstream turbine that maximizes the overall power production of both turbines. For wind speed = 10 m/s, wind direction = 90° and spacing = 4D, this graphical method resulted in the generation of the two plots in Fig. 5.6 and Fig. 5.7.

3D Surface Plot of Total Power vs Yaw and Derating
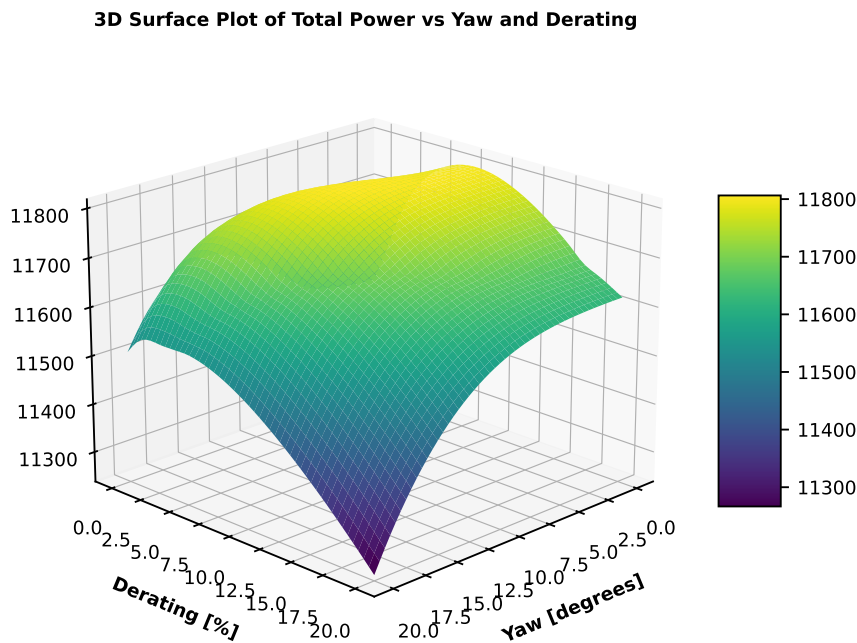
Figure 5.6: 3D Surface plot from the parametric analysis.

Initial guess: 15 degrees of yaw and 10% derating			
Spacing	Derating [%]	Yaw [deg]	Power [kW]
3D	11.2	7.9	11077.7
4D	6.0	8.8	11805.4
5D	4.4	12.7	12496.7
6D	2.3	12.0	13150.4

Initial guess: 10 degrees of yaw and 15% derating			
Spacing	Derating [%]	Yaw [deg]	Power [kW]
3D	7.9	13.5	11009.3
4D	3.9	14.1	11764.3
5D	0.0	12.1	12428.3
6D	0.0	13.2	13120.5

Initial guess: 8 degrees of yaw and 20% derating			
Spacing	Derating [%]	Yaw [deg]	Power [kW]
3D	11.4	6.2	11084.4
4D	7.1	7.7	11806.5
5D	5.4	11.5	12496.3
6D	2.5	10.7	13151.2

Initial guess: 5 degrees of yaw and 25% derating			
Spacing	Derating [%]	Yaw [deg]	Power [kW]
3D	11.7	4.2	11090.0
4D	3.9	12.6	11782.9
5D	4.3	8.2	12482.3
6D	4.4	7.0	13133.3

Initial guess: 0 degrees of yaw and 30% derating			
Spacing	Derating [%]	Yaw [deg]	Power [kW]
3D	13.1	0.0	11092.9
4D	7.6	2.5	11798.7
5D	5.5	2.5	12468.5
6D	5.3	2.4	13108.0

Table 5.6: Multi-start method simulations. Derating and yaw values are referred to the upstream turbine.

Contour Plot of Total Power vs Yaw and Derating
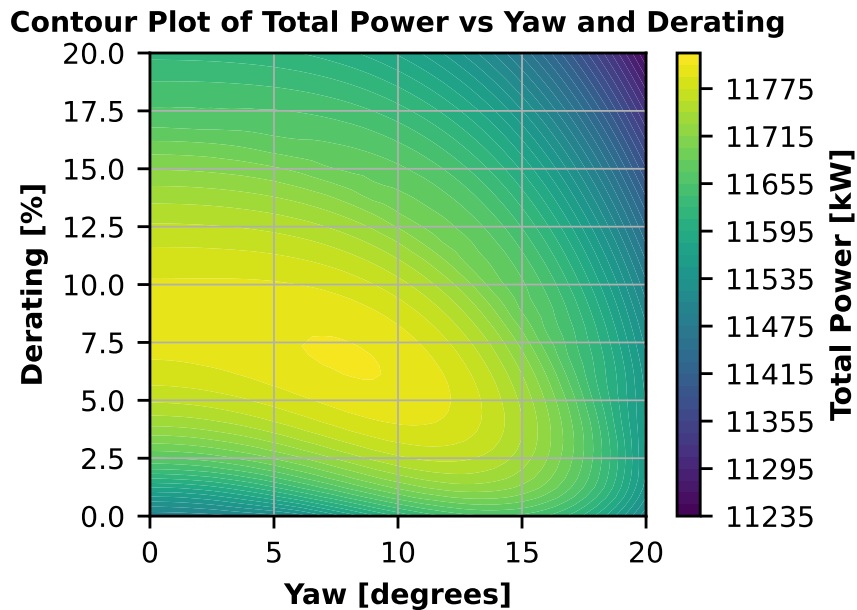
Figure 5.7: Contour plot from the parametric analysis.

The best yaw and derating pair obtained with the multi-start method at 4D corresponds to 7.1% derating and 7.7 degrees of misalignment, which fall precisely within the yellow area in Fig. 5.7. These analyses led to the conclusion that if the optimization problem were integrated with an additional objective such as that of load minimization the optimization process would not encounter local minima or at least would be more robust. Also, if the optimization were based on a gradient-based method such as SLSQP[4], instead of COBYLA, and were paired with the calculation of the analytical gradient, the global optimum would be easier to identify.

5.2.5. Comparison between controlled wind farm and baseline case

Notwithstanding the numerical issues, the simulations run with the synergistic approach of derating and wake redirection show higher power outcomes that are now compared with the other strategies and the baseline case. The results displayed in Table 5.7 refer to the array of wind speed [7, 8, 9, 10] m/s and to a spacing of 4D, to be consistent with the reference spacing used so far.

---

[4]SLSQP stands for Sequential Least Squares Programming.

Wind speed = 7 m/s		
	Power output [kW]	% Increase compared to base case
Baseline	3648.8	-
Derating only	3977.9	9.0
WR only	3920.1	7.4
Derating+WR	4015.4	10.0

Wind speed = 8 m/s		
	Power output [kW]	% Increase compared to base case
Baseline	5547.6	-
Derating only	5965.8	7.5
WR only	5898.9	6.3
Derating+WR	6019.8	8.5

Wind speed = 9 m/s		
	Power output [kW]	% Increase compared to base case
Baseline	8045.1	-
Derating only	8506.7	5.7
WR only	8412.1	4.6
Derating+WR	8545.2	6.2

Wind speed = 10 m/s		
	Power output [kW]	% Increase compared to base case
Baseline	11493.5	-
Derating only	11797.3	2.6
WR only	11654.3	1.4
Derating+WR	11806.5	2.7

Table 5.7: Comparison of power outputs across strategies at 4D.

The trend observed suggests that while the combination of derating and wake redirection generally provides the highest increase in power output, the incremental benefits decrease as wind speed increases. This is very evident from the plot in Fig. 5.8, which represents the nominal power curve alongside the percentage increases for all wind speeds from cut-in to cut-out. The peak gain in power capture is achieved at 7 m/s and is equal to 10%, which is a very promising value and aligns with the outcomes present in literature (refer to [6, 16, 29] for similar studies).
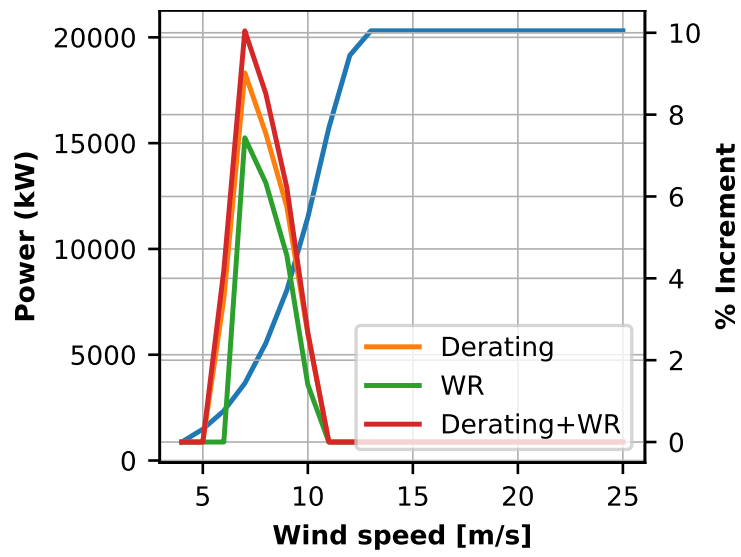
Figure 5.8: Baseline power curve and percentage increments for each control strategy.

6 | Conclusions and future developments

The findings illustrated a promising potential for the combined control strategy to increase power production by up to 10.0%, though variations were observed based on wind speed. This reinforced the effectiveness of an integrated approach and the importance of considering the wind farm as a cohesive system rather than a collection of independent turbines.

However, the thesis also acknowledges the limitations inherent in the study, including simulations based on a single inflow condition, a simple layout and a stationary wind direction. It suggests that future research should encompass multiple inflow scenarios and more complex wind farm geometries to validate the robustness of the results and develop closed-loop control systems responsive to the dynamic nature of wind conditions, ensuring the strategies' applicability to actual wind farm operations.

Furthermore, this work has laid the groundwork for further exploration. Future research is expected to expand into comparative analyses of other wake redirection methods such as Individual Pitch Control (IPC) and tilt-based WR, as well as in the potential enhancements achievable through strategic turbine repositioning within the farm layout. Last but not least the future progression of this research ought to include the integration of load minimization and economic optimization among the work's objectives, to assess the monetary advantages of various wind farm control strategies and their impact on turbines' structural integrity and subsequent maintenance costs.

Ultimately, it would be of great interest to classify with a systematic approach the best practices for control strategy combinations, tailored to the specific conditions of real-world settings. This will contribute to maximized energy production, minimized structural loading, and reduced wake-induced power losses, aligning with the global move toward a more sustainable and resilient energy infrastructure.

Bibliography

[1] Iea-10.0-198-rwt. URL `https://github.com/IEAWindTask37/IEA-10.0-198-RWT/blob/f4c09ba7b1d4481156eb35394bf1276b5d250ba6/hawc2/hawcstab2/steadystate_modal.htc#L147`.

[2] *Aerodynamics of Wind Turbines*, chapter 3, pages 91–155. John Wiley Sons, Ltd, 2009. ISBN 9781119994367. doi: https://doi.org/10.1002/9781119994367.ch3.

[3] N. 2019. Floris. version 1.0.0. URL `https://github.com/NREL/floris`.

[4] L. E. Andersson, O. Anaya-Lara, J. O. Tande, K. O. Merz, and L. Imsland. Wind farm control - Part I: A review on control system concepts and structures. *IET Renewable Power Generation*, 15(10):2085–2108, 2021. ISSN 1752-1424. doi: 10.1049/rpg2.12160.

[5] J. Annoni, P. Fleming, A. Scholbrock, J. Roadman, S. Dana, C. Adcock, F. Porte-Agel, S. Raach, F. Haizmann, and D. Schlipf. Analysis of control-oriented wake modeling tools using lidar field results. *Wind Energy Science*, 3(2):819–831, Nov. 2018. ISSN 2366-7443. doi: 10.5194/wes-3-819-2018. Publisher: Copernicus GmbH.

[6] R. K. Balakrishnan and S.-h. Hur. Maximization of the power production of an offshore wind farm. *Applied Sciences*, 12(8), 2022. ISSN 2076-3417. doi: 10.3390/app12084013.

[7] C. J. Bay, P. Fleming, B. Doekemeijer, J. King, M. Churchfield, and R. Mudafort. Addressing deep array effects and impacts to wake steering with the cumulative-curl wake model. *Wind Energy Science*, 8(3):401–419, Mar. 2023. ISSN 2366-7443. doi: 10.5194/wes-8-401-2023. Publisher: Copernicus GmbH.

[8] S. Boersma, B. Doekemeijer, P. Gebraad, P. Fleming, J. Annoni, A. Scholbrock, J. Frederik, and J.-W. van Wingerden. A tutorial on control-oriented modeling and control of wind farms. In *2017 American Control Conference (ACC)*, pages 1–18, May 2017. doi: 10.23919/ACC.2017.7962923. ISSN: 2378-5861.

[9] P. Bortolotti, H. Tarrés, K. Dykes, K. Merz, L. Sethuraman, D. Verelst, and F. Zahle.

IEA Wind TCP Task 37: Systems Engineering in Wind Energy-WP2.1 Reference Wind Turbines. National Renewable Energy Laboratory (NREL), 2019. doi: 10.2172/1529216.

[10] R. Busby. *Wind Power: The Industry Grows Up.* PennWell Corporation, 2012. ISBN 9781593702441. URL `https://books.google.it/books?id=-tzo7QXuHfMC`.

[11] A. Crespo, J. Hernández, and S. Frandsen. Survey of modelling methods for wind turbine wakes and wind farms. *Wind Energy*, 2(1):1–24, 1999. ISSN 1099-1824. doi: 10.1002/(SICI)1099-1824(199901/03)2:1<1::AID-WE16>3.0.CO;2-7.

[12] A. Croce, S. Cacciola, and F. Isella. Combining wake redirection and derating strategies in a wind farm load-constrained power maximization. *Wind Energy Science Discussions*, 2023:1–27, 2023. doi: 10.5194/wes-2023-145.

[13] R. Damiani, S. Dana, J. Annoni, P. Fleming, J. Roadman, J. van Dam, and K. Dykes. Assessment of wind turbine component loads under yaw-offset conditions. *Wind Energy Science*, 3(1):173–189, 2018. doi: 10.5194/wes-3-173-2018.

[14] DTU. Hawcstab2. URL `https://www.hawcstab2.vindenergi.dtu.dk`.

[15] DTU Wind Energy. Pywake. version 2.5.0. URL `https://topfarm.pages.windenergy.dtu.dk/PyWake`.

[16] P. Fleming, P. M. Gebraad, S. Lee, J.-W. van Wingerden, K. Johnson, M. Churchfield, J. Michalakes, P. Spalart, and P. Moriarty. Simulation comparison of wake mitigation control strategies for a two-turbine case. *Wind Energy*, 18(12):2135–2143, 2015. doi: https://doi.org/10.1002/we.1810.

[17] T. M. Fletcher and R. E. Brown. Simulation of wind turbine wake interaction using the vorticity transport model. *Wind Energy*, 13(7):587–602, 2010. doi: https://doi.org/10.1002/we.379.

[18] F. Gori, S. Laizet, and A. Wynn. Sensitivity analysis of wake steering optimisation for wind farm power maximisation. *Wind Energy Science*, 8(9):1425–1451, Sept. 2023. ISSN 2366-7443. doi: 10.5194/wes-8-1425-2023. Publisher: Copernicus GmbH.

[19] M. H. Hansen. Aeroelastic properties of backward swept blades. January 4–7 2011. doi: https://doi.org/10.2514/6.2011-260. Paper Number AIAA 2011-260.

[20] C. Hasager, L. Rasmussen, A. Peña, L. Jensen, and P.-E. Réthoré. Wind farm wake: The horns rev photo case. *Energies*, 6:696–716, 02 2013. doi: 10.3390/en6020696.

[21] IEA. Electricity generation mix, denmark, 2022, 2022. URL `https://www.iea.org/countries/denmark`.

[22] IEA. Renewables 2023, iea, paris, 2024. URL `https://www.iea.org/reports/renewables-20237`.

[23] IRENA. Renewable capacity statistics 2023, international renewable energy agency, abu dhabi., 2023. URL `https://mc-cd8320d4-36a1-40ac-83cc-3389-cdn-endpoint.azureedge.net/-/media/Files/IRENA/Agency/Publication/2023/Mar/IRENA_RE_Capacity_Statistics_2023.pdf?rev=d2949151ee6a4625b65c82881403c2a7`.

[24] N. Jensen. *A note on wind generator interaction*. Number 2411 in Risø-M. Risø National Laboratory, 1983. ISBN 87-550-0971-9.

[25] Jiménez, A. Crespo, and E. Migoya. Application of a les technique to characterize the wake deflection of a wind turbine in yaw. *Wind Energy*, 13(6):559–572, 2010. doi: https://doi.org/10.1002/we.380.

[26] A. C. Kheirabadi and R. Nagamune. A quantitative review of wind farm control with the objective of wind farm power maximization. *Journal of Wind Engineering and Industrial Aerodynamics*, 192:45–73, Sept. 2019. ISSN 0167-6105. doi: 10.1016/j.jweia.2019.06.015.

[27] J. King, P. Fleming, R. King, L. A. Martínez-Tossas, C. J. Bay, R. Mudafort, and E. Simley. Control-oriented model for secondary effects of wake steering. *Wind Energy Science*, 6(3):701–714, May 2021. ISSN 2366-7443. doi: 10.5194/wes-6-701-2021. Publisher: Copernicus GmbH.

[28] P. K. Kundu, I. M. Cohen, and D. R. Dowling. Chapter 4 - conservation laws. In P. K. Kundu, I. M. Cohen, and D. R. Dowling, editors, *Fluid Mechanics (Sixth Edition)*, pages 109–193. Academic Press, Boston, sixth edition edition, 2016. ISBN 978-0-12-405935-1. doi: https://doi.org/10.1016/B978-0-12-405935-1.00004-6.

[29] B. Li, J. He, M. Ge, H. Ma, B. Du, H. Yang, and Y. Liu. Study of three wake control strategies for power maximization of offshore wind farms with different layouts. *Energy Conversion and Management*, 268:116059, 2022. ISSN 0196-8904. doi: https://doi.org/10.1016/j.enconman.2022.116059.

[30] W. H. Lio, M. Mirzaei, and G. C. Larsen. On wind turbine down-regulation control strategies and rotor speed set-point. *Journal of Physics: Conference Series*, 1037(3): 032040, jun 2018. doi: 10.1088/1742-6596/1037/3/032040.

[31] P. B. S. Lissaman. Energy Effectiveness of Arbitrary Arrays of Wind Turbines. *Journal of Energy*, 3(6):323–328, Nov. 1979. ISSN 0146-0412. doi: 10.2514/3.62441. Publisher: American Institute of Aeronautics and Astronautics.

[32] D. Medici, S. Ivanell, J.- Dahlberg, and P. H. Alfredsson. The upstream flow of a wind turbine: blockage effect. *Wind Energy*, 14(5):691–697, 2011. ISSN 1099-1824. doi: 10.1002/we.451.

[33] F. Meng, A. W. H. Lio, and J. Liew. The effect of minimum thrust coefficient control strategy on power output and loads of a wind farm. *Journal of Physics: Conference Series*, 1452(1):012009, jan 2020. doi: 10.1088/1742-6596/1452/1/012009.

[34] A. Niayifar and F. Porté-Agel. Analytical modeling of wind farms: A new approach for power prediction. *Energies*, 9(9), 2016. ISSN 1996-1073. doi: 10.3390/en9090741.

[35] K. Nilsson, S. Ivanell, K. S. Hansen, R. Mikkelsen, J. N. Sørensen, S.-P. Breton, and D. Henningson. Large-eddy simulations of the Lillgrund wind farm. *Wind Energy*, 18(3):449–467, 2015. ISSN 1099-1824. doi: 10.1002/we.1707.

[36] M. M. Pedersen, P. van der Laan, M. Friis-Møller, J. Rinker, and P.-E. Réthoré. Dtuwindenergy/pywake: Pywake, Feb. 2019. URL `https://doi.org/10.5281/zenodo.2562662`.

[37] F. Porté-Agel, M. Bastankhah, and S. Shamsoddin. Wind-Turbine and Wind-Farm Flows: A Review. *Boundary-Layer Meteorology*, 174(1):1–59, Jan. 2020. ISSN 1573-1472. doi: 10.1007/s10546-019-00473-0.

[38] R. Riva, J. Liew, M. Friis-Møller, N. Dimitrov, E. Barlas, P.-E. Réthoré, and A. Beržonskis. Wind farm layout optimization with load constraints using surrogate modelling. *Journal of Physics: Conference Series*, 1618(4):042035, sep 2020. doi: 10.1088/1742-6596/1618/4/042035. URL `https://dx.doi.org/10.1088/1742-6596/1618/4/042035`.

[39] C. Shapiro, D. Gayme, and C. Meneveau. Modelling yawed wind turbine wakes: A lifting line approach. *Journal of Fluid Mechanics*, 841, 04 2018. doi: 10.1017/jfm.2018.75.

[40] Tao, Z. Xu, A. E. Feijoo, Kuenzel, and N. Bokde. Integrated wind farm power curve and power curve distribution function considering the wake effect and terrain gradient. *Energies*, 12:2482, 06 2019. doi: 10.3390/en12132482.

[41] The OpenMDAO Development Team. Explicitcomponent. URL `https:`

`//openmdao.org/newdocs/versions/latest/features/core_features/`
`working_with_components/explicit_component.html`.

[42] D. Vahidi and F. Porté-Agel. A physics-based model for wind turbine wake expansion in the atmospheric boundary layer. *Journal of Fluid Mechanics*, 943:A49, 2022. doi: 10.1017/jfm.2022.443.

[43] J. A. Vitulli, G. C. Larsen, M. M. Pedersen, S. Ott, and M. Friis-Møller. Optimal open loop wind farm control. *Journal of Physics: Conference Series*, 1256(1):012027, July 2019. ISSN 1742-6596. doi: 10.1088/1742-6596/1256/1/012027. Publisher: IOP Publishing.

[44] H. Zong and F. Porté-Agel. A momentum-conserving wake superposition method for wind farm power prediction. *Journal of Fluid Mechanics*, 889:A8, 2020. doi: 10.1017/jfm.2020.77.

A | Appendix A

3D Surface Plot of Total Power vs Yaw and Derating
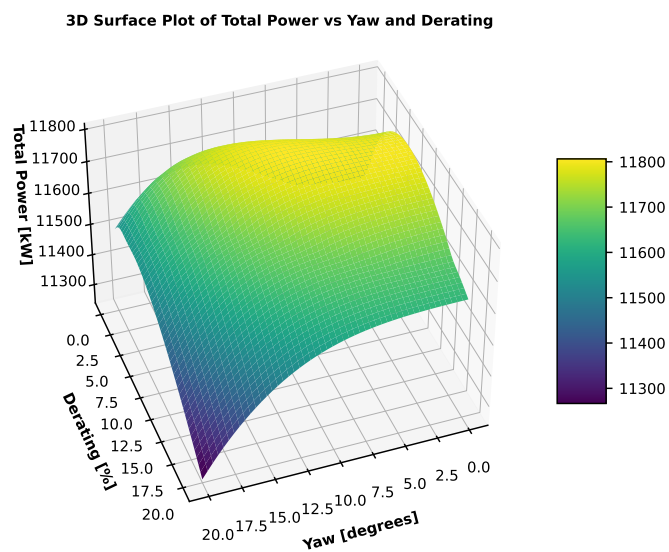
Figure A.1: 3D Surface plot from the parametric analysis.
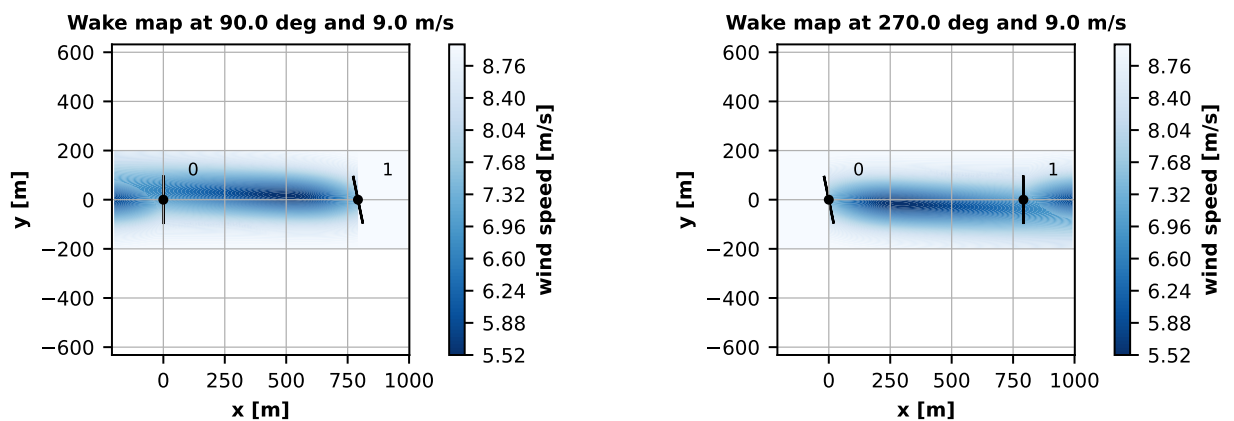
Figure A.2: Wake maps for the combined strategy at 90° (left) and 270° (right) at 9 m/s, with a 4D spacing. The upstream turbine is yawed by 11.6 degrees and derated by 4%.

List of Figures

List of Tables

List of Symbols

Variable	Description	SI unit
a	Axial induction factor	-
u	Streamwise velocity component	m/s
u_∞	Freestream velocity	m/s
δu	Velocity deficit	m/s
C_T	Thrust coefficient	-
C_P	Power coefficient	-
β	Blade pitch angle	degrees
ω	Rotor speed	rpm
λ	Tip speed ratio	-
DEL	Damage Equivalent Load	kNm